Intracellular Delivery of Proteins in Complexes with Oligoarginine-Modified Liposomes and the Effect of Oligoarginine Length

Masahiko Furuhata,[†] Hiroko Kawakami,[‡] Kazunori Toma,[‡] Yoshiyuki Hattori,[†] and Yoshie Maitani*[,†]

Institute of Medicinal Chemistry, Hoshi University, Shinagawa-ku, Tokyo 142-8501, Japan, and The Noguchi Institute, Itabashi-ku, Tokyo 173-0003, Japan. Received February 13, 2006; Revised Manuscript Received June 5, 2006

The intracellular delivery of proteins using cell-penetrating peptides (CPPs) including oligoarginine (oligo-Arg) carriers raises the possibility of establishing novel therapeutic methods. We compared the effect of the length of oligo-Arg in modified liposomes ($(Arg)_n$-L; n = 4, 6, 8, 10) on the delivery of proteins by flow cytometry, fluorescence microscopy, and spectrofluorimetry. As a free liposome, Arg4-modified liposome Arg4-L was most efficiently internalized in cells. The efficiency decreased depending on the length of oligo-Arg. For the intracellular delivery of proteins, $(Arg)_n$-L was physically associated with proteins. Concerning the effect of oligo-Arg length, liposome/protein complexes showed a different behavior. Arg4-L carried bovine serum albumin (BSA, 66 kDa) and β-galactosidase (β-Gal, 120 kDa) 6-fold higher than free BSA and free β-Gal. Arg10-L showed similar performance for these two proteins to Arg4-L. The enzymatic activity of β-Gal in the cells showed that proteins were transported as a biologically active form. Arg10-L carried 100-fold more immunoglobulin G (IgG, 150 kDa) than free IgG, and 3-fold more than Arg4-L into cells. Shorter oligo-Arg chain on liposomes may be enough for liposomes alone to be taken up in cells, but more Arg residues may be needed to form a complex with high molecular weight proteins and deliver them into cells. This information will aid in the design of $(Arg)_n$-L as a carrier for delivering proteins into cells.

INTRODUCTION

The development of therapeutic peptides and proteins is hampered by their poor ability to penetrate the plasma membrane because of their high hydrophilicity and molecular weight. Therefore, it is necessary to construct an efficient protein delivery system. One approach to solve this problem is to incorporate short peptides derived from protein-transduction domains (PTDs) or cell-penetrating peptides (CPPs), such as HIV-1 Tat fragments, penetratin and VP22. PTDs or CPPs are less than 30 amino acid residues in length and have the capability of crossing the plasma membrane (*1*−*6*). Since the PTDs and CPPs can deliver conjugated molecules, such as proteins, into cells (*7*, *8*), they are usually used as conjugates with cargo molecules, as part of a very strong and specific complex with biotin (*9*). However, these CPP carriers require cross-linking to the target peptide or protein. The only exception is pep-1, which has been reported to deliver a variety of peptides and proteins into several cell lines by forming physical assemblies without covalent chemical coupling (*6*). Since CPP-modified nanoparticles (*10*) and liposomes (*11*) can be taken up into cells, liposomes modified with Tat and penetratin were utilized in the intracellular delivery of drugs by entrapping the drugs in the liposomes (*12*). However, in the case of proteins, it is hard for them to be released from the liposomes, even if the liposomes are internalized in cells.

We synthesized oligo-Arg conjugates with an artificial lipid, and they were incorporated in liposomes for a protein delivery study. In our system, the surface of liposomes were modified with oligo-Arg ($(Arg)_n$-L; n = 4, 6, 8, 10), and proteins were physically associated on the surface. Cargo proteins were not entrapped in the liposomes. Therefore, the preparation of the complex between proteins and $(Arg)_n$-L is simple. Although investigations delineating the influence of Arg length on the uptake of oligo-Args alone have been reported (*5*, *13*−*15*), to our knowledge there is no report on $(Arg)_n$-L as a protein delivery system. $(Arg)_n$-L provides two characteristic interactions; a hydrophobic one by liposome, and a positively charged and hydrophilic one by (Arg)n. These two kinds of interactions were expected to help forming complexes with proteins.

The aim of this study is first to show that our system can transport proteins into cells, and then to examine the effect of oligo-Arg length on the protein delivery in human cervical carcinoma HeLa cells. Cellular uptake efficacy was evaluated by flow cytometry, spectrofluorimetry, and fluorescence microscopic observation of the cells. We also analyzed the interaction of $(Arg)_n$-L with proteins by fluorescence intensity distribution analysis (FIDA).

Our studies showed that the effect of oligo-Arg length on the intracellular delivery of proteins by $(Arg)_n$-L/protein complexes was different from that of $(Arg)_n$-L alone. Short oligo-Arg was enough for liposomes to be taken up into the cells, but longer oligo-Arg may be needed to form a complex with large proteins and deliver them into the cells.

EXPERIMENTAL PROCEDURES

Materials. All amino acid derivatives and coupling reagents were obtained from Kokusan Chemical Co., Ltd. (Tokyo, Japan). Egg phosphatidylcholine (EPC) was purchased from Q. P. Co., Ltd. (Tokyo, Japan). Cholesterol (Chol) and bovine serum albumin (BSA) were purchased from Wako Pure Chemical Industries, Ltd. (Osaka, Japan). Calcein was obtained from Tokyo Kasei Kogyo Co., Ltd. (Tokyo, Japan). Fluorescein isothiocyanate-labeled BSA (FITC−BSA), stearylamine, 3β-[*N*-(dimethylaminoethane)carbamoyl]cholesterol (DC−Chol), 5-(*N*-ethyl-*N*-isopropyl)amiloride (EIPA), phorbol 12-myristate 13-acetate (PMA) were from Sigma Chemical Co. (St. Louis, MO). FITC-immunoglobulin G (FITC−IgG) was provided by

* Corresponding author. Fax/phone: +81-3-5498-5048; e-mail: yoshie@hoshi.ac.jp.

[†] Hoshi University.

[‡] The Noguchi Institute.

10.1021/bc060034h CCC: $33.50
Published on Web 07/06/2006

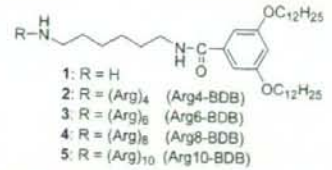

Figure 1. Chemical structures of $(Arg)_n$-BDBs.

MP Biomedicals Co. (Irvine, CA). IgG was obtained from Oriental Yeast Co., Ltd. (Tokyo, Japan). β-Galactosidase (β-Gal) and the β-Gal staining kit were purchased from Active Motif, Inc. (Carlsbad, CA). Lumi-Gal 530 (Reporter assay kit of β-Gal) was from Toyobo Co., Ltd. (Osaka, Japan). Bicinchonic acid (BCA) protein assay reagent was obtained from Pierce (Rockford, IL). Dulbecco's modified Eagle's medium (DMEM) was purchased from Invitrogen Co. (Carlsbad, CA). Fetal bovine serum (FBS) was provided by Life Technologies (Grand Island, NY). 1,1′-Dioctadecyl-3,3,3′,3′-tetramethylindocarbocyanine perchlorate (DiI) was obtained from Lambda Probes & Diagnostics (Graz, Austria). All other reagents were of analytical grade.

Synthesis of $(Arg)_n$-BDBs. $(Arg)_n$-BDBs (**2**, **3**, **4**, and **5**) were synthesized similarly to other peptide−lipid conjugates of different amino acid sequences (*16*) (Figure 1). The oligo-Arg portion was extended similarly to the compounds with a PEG linker between oligo-Arg and BDB (*17*). For example, N^{α}-9-fluorenylmethoxycarbonyl-N^{g}-2,2,5,7,8-pentamethylchroman-6-sulfonyl-L-arginine (Fmoc-Arg(Pmc)-OH) was condensed with *N*-(6-aminohexyl)-3,5-bis(dodecyloxy)benzamide (**1**) by 2-(1*H*-benzotriazol-1-yl)-1,1,3,3-tetramethyluronium hexafluorophosphate and 4-(dimethylamino)pyridine in *N*,*N*-dimethylformamide, and the Fmoc protecting group was removed by piperidine. This amide condensation and Fmoc deprotection cycle was repeated four times to give the side chain protected **2**. MALDI-TOFMS (α-CHCA): found, 2280.24; calculated for $[M + H]^+$, 2278.33. Final trifluoroacetic acid deprotection of Pmc gave **2**. MALDI-TOFMS (α-CHCA): found, 1214.99; calculated for $[M + H]^+$, 1213.94.

Cell Culture. HeLa cells were kindly provided by Toyobo Co., Ltd. (Osaka, Japan). HeLa cells were grown in DMEM supplemented with 10% FBS at 37 °C in a humidified 5% CO_2 atmosphere.

Preparation of Liposomes. Four liposomal formulas were used: EPC, Chol, and $(Arg)_n$-BDB in a molar ratio of 7:3:0.05 or 7:3:0.5 for the oligo-Arg-modified liposome ($(Arg)_n$-L); EPC and Chol in a molar ratio of 7:3 for the control liposome (Con-L); EPC, Chol, and stearylamine in a molar ratio of 7:3:2 for the stearylmaine modified liposome (SA-L); EPC, Chol, and DC−Chol in a molar ratio of 7:3:0.5 for the DC−Chol modified liposome (DC-L) for the control liposomes containing cationic lipids. Liposomes were prepared by a dry film method with water or 20 mM calcein. For $(Arg)_n$-L, $(Arg)_n$-BDB, Chol, and EPC were dissolved in an appropriate volume of chloroform, which was then removed. The particle size distributions and the zeta-potentials were measured by the dynamic and the electrophoresis light scattering method, respectively (ELS-800, Otsuka Electronics Co., Ltd., Osaka, Japan), at 25°C, after the dispersion was diluted to an appropriate volume with water. pH titration of the zeta-potential was measured by Automatic Titrator GT-06 (Mitsubishi Chemical Corporation, Tokyo, Japan). For liposomes with calcein entrapped, this was followed by chromatography on Sephadex G-50 columns, and fractions of liposomes were collected. DiI-labeled liposomes were prepared as described above but with post-addition of DiI at 0.04 mol % of total lipids.

Uptake Experiments Using Flow Cytometry. An aqueous solution of FITC−BSA, FITC−IgG, or β-Gal was added to the $(Arg)_n$-L suspension with gentle shaking to form $(Arg)_n$-L/protein complexes. Each complex was left at room temperature for 10−15 min. Cell cultures were prepared by plating cells in a 35-mm culture dish 24 h prior to each experiment. The cells were washed three times with 1 mL of serum-free DMEM. Calcein-entrapped $(Arg)_n$-L (100 μg) alone or each $(Arg)_n$-L/protein complex ($(Arg)_n$-BDB: 5 μg of protein, from 50:1 to 1000:1 molar ratio), was diluted with serum-free DMEM to 1 mL and then gently applied to the cells. In this study, all samples were incubated with cells for 3 h at 37 °C in serum-free DMEM. At the end of the incubation of $(Arg)_n$-L/protein complexes or calcein-entrapped $(Arg)_n$-L with cells, the cells were washed three times with 1 mL of PBS and detached by incubating with 0.05% trypsin and EDTA solution at 37 °C for 3 min. The cells were centrifuged at 1500*g*, and the supernatant was discarded. The cells were resuspended with PBS (pH 7.4) containing 0.1% BSA and 1 mM EDTA and directly introduced into a FACS-Calibur flow cytometer (Becton Dickinson, San Jose, CA) equipped with a 488 nm argon ion laser. Data for 10000 fluorescent events were obtained by recording forward scatter (FSC) and side scatter (SSC) with green (for FITC and calcein; 530/30 nm) and red (for DiI; 585/42 nm) fluorescence. To investigate the cellular uptake mechanism, cells were washed with serum-free medium and preincubated for 30 min at 37 °C with EIPA (25 μM) or PMA (1 μM). Subsequent incubation of the complex was carried out in the presence of the respective pharmacological reagents.

Spectrofluorimetric Quantification of Internalized FITC−BSA and IgG. At the end of the incubation of $(Arg)_n$-L/FITC-protein complexes with cells as described above, the cells were washed three times with 1 mL of PBS and lysed by incubating with 0.2% Triton X-100/PBS at 37 °C for 5 min, followed by centrifugation at 15000 rpm for 15 min. The supernatants were measured with a chemoluminometer (Ex = 485, Em = 535 nm) (Wallac ARVO SX 1420 multilabel counter, Perkin-Elmer Life Science, Japan, Co. Ltd., Kanagawa, Japan).

Fluorescence Microscopy. At the end of the incubation of $(Arg)_n$-L/protein complexes with cells as described in Uptake Experiments using Flow Cytometry, the cells were washed five times with 1 mL of PBS. Unfixed cells were observed with an Eclipse TS100/100-F for epifluorescence observations (Nicon, Tokyo, Japan). The level of contrast and the brightness of the images were adjusted.

***β*-Galactosidase Assay.** For the β-galactosidase assay, we used X-Gal staining and chemiluminescence measurements. For X-Gal staining, at the end of the incubation of $(Arg)_n$-L/β-Gal complex with cells as described in Uptake Experiments using Flow Cytometry, the cells were stained with the β-Gal staining kit and then observed with an Eclipse TS100/100-F for epifluorescence observations. The level of contrast and the brightness of the images were adjusted. For chemiluminescence measurements, β-Gal activity was measured according to the instructions accompanying the β-Gal assay system. Incubation of $(Arg)_n$-L/β-Gal complex with cells was terminated by washing the plates three times with cold PBS (pH 7.4). Cell lysis solution (Reporter assay kit of β-Gal) was added to the cell monolayers and subjected to freezing at −80 °C and thawing at 37 °C, followed by centrifugation at 15000 rpm for 2 min. Aliquots of 20 μL of the supernatants were mixed with 180 μL of Lumi-Gal 530 and then incubated for 30 min at 37 °C, and counts per second (cps) were measured with a chemoluminometer (Wallac ARVO SX 1420 multilabel counter). The protein concentration of the supernatants was determined with BCA reagent using BSA as a standard, and cps/μg protein was calculated.

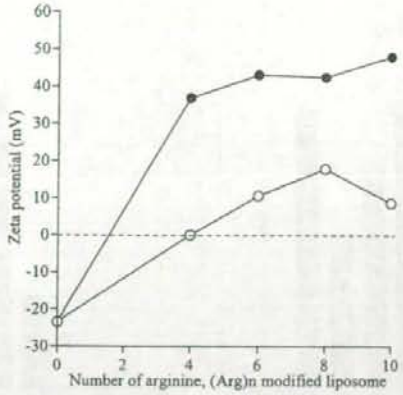

Figure 2. Effect of arginine number of $(Arg)_n$-L on the zeta potential. Open circle, liposome contained 0.5 mol % of oligo-Arg-BDB; Closed circle, liposome contained 5 mol % of oligo-Arg-BDB

Fluorescence Intensity Distribution Analysis (FIDA). FIDA was performed with a MF20 microplate reader (Olympus Corp. Tokyo, Japan) using the onboard 633-nm helium−neon laser at a power of 300 μW for excitation. Experiments were performed in 384-well glass-bottom plates using a sample volume of 50 μL. The FIDA data was analyzed with the MF20 software package. All single-molecule FIDAs were performed under identical conditions with respect to incubation (10 min) at room temperature. Protein-binding experiments were performed using the DiI-labeled Arg4-L and Arg10-L. The concentration of the labeled component was held constant whereas the concentration of BSA or IgG was varied in water.

Cytotoxicity. HeLa cells were seeded at a density of 1×10^4 cells per well in 96-well plates and maintained for 24 h before transfection in DMEM supplemented with 10% FBS. The cells were washed with PBS. The culture medium was replaced with serum-free DMEM (100 μL) including $(Arg)_n$-L/protein complex ($(Arg)_n$-BDB: 5 μg of protein = 50:1, molar ratio). After incubation for 3 h at 37 °C with serum-free DMEM (100 μL), the number of surviving cells was determined by a WST-8 assay (Dojindo Laboratories, Kumamoto, Japan). Cell viability was expressed as the ratio of the A_{450} of cells treated with the protein complex to that of the control samples.

Data Analysis. Significant differences in the mean values were evaluated using Student's unpaired *t*-test. A *p*-value of less than 0.05 was considered significant.

RESULTS

Characterization of $(Arg)_n$-L. We prepared five kinds of liposomes; a control liposome (Con-L) consisting of EPC and Chol at a molar ratio of 7:3, two positively charged control liposomes consisting of EPC, Chol, stearylamine or DC−Chol at a molar ratio of 7:3:2 or 0.5 (SA-L, DC-L, respectively), and two $(Arg)_n$-L ($n = 4, 6, 8, 10$) differing in $(Arg)_n$-BDB content, a molar ratio of EPC, Chol, and $(Arg)_n$-BDB at 7:3:0.05 and 7:3:0.5. Each particle size was adjusted to about 200 nm by sonication. To examine whether the liposomes were modified with Arg, we measured their zeta potential. Con-L was negatively charged, and the two $(Arg)_n$-L were positively charged (Figure 2). SA-L and DC-L were positively charged (over 50 mV in zeta potential, data not shown). The longer oligo-Arg had a higher zeta-potential, corresponding to the number of Arg residues. The zeta-potential of $(Arg)_n$-L containing 5 mol % of oligo-Arg lipid was higher than that of preparation containing 0.5 mol % (Figure 2). We used $(Arg)_n$-L containing 5 mol % of oligo-Arg lipid in the subsequent experiments, because we thought that highly positively charged carriers were desirable to form complexes with proteins and to deliver them into cells.

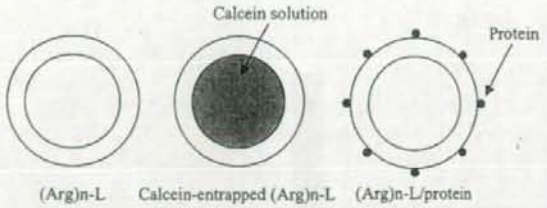

Figure 3. Schematic diagrams of the $(Arg)_n$-L, calcein-entrapped $(Arg)_n$-L and $(Arg)_n$-L/protein complex. ($(Arg)_n$-BDB in $(Arg)_n$-L): protein = 50:1, molar ratio.

Cellular Uptake of Calcein-Entrapped $(Arg)_n$-L, and $(Arg)_n$-L/FITC−BSA, and $(Arg)_n$-L/FITC−IgG Complexes. To examine the cellular uptake of $(Arg)_n$-L or the complex, cells were exposed to calcein-entrapped $(Arg)_n$-L alone, and $(Arg)_n$-L/FITC−BSA and $(Arg)_n$-L/FITC−IgG complexes for 3 h at 37 °C. Then, the cells were trypsinized and analyzed by flow cytometry. The cellular uptake of calcein-entrapped $(Arg)_n$-L decreased as the number of arginine residues increased (Figure 4A). The size of Arg4-L and Arg10-L was about 233 nm. The size of Arg4-L/FITC−BSA and FITC−IgG, and Arg10-L/FITC−BSA and FITC−IgG was about 289 nm, indicating that proteins were adhered to the surface of liposomes as schematically shown in Figure 3. The zeta potential of Arg10-L/BSA and Arg10-L/IgG was similar to that of Arg10-L at pH 3−11 when measured by the pH titration method (data not shown).

Free FITC−BSA, Con-L/FITC−BSA, SA-L/FITC−BSA, and DC-L/FITC−BSA were scarcely taken into the cell (Figure 4B). FITC−BSA in a complex with Arg4-L, Arg6-L, Arg8-L, and Arg10-L displayed a marked increase in fluorescence in the cells, showing about a 6-, 5-, 3-, and 6-fold higher intensity, respectively, than free FITC−BSA. Arg4-L and Arg10-L were most efficient at delivering FITC−BSA into the cells.

Free FITC−IgG (150 kDa), Con-L/FITC−IgG, SA-L/FITC−IgG, and DC-L/FITC−IgG complexes were scarcely taken up at all (Figure 4C). FITC−IgG in a complex with Arg4-L, Arg6-L, Arg8-L, and Arg10-L showed about 30-, 100-, 60-, and 100-fold greater cellular uptake, respectively, than free FITC−IgG. Arg6-L and Arg10-L showed the greatest efficiency in delivering FITC−IgG. However, FITC−IgG and Arg10-L without complex formation showed less cellular uptake of FITC−IgG than Arg4-L/FITC−IgG (data not shown).

We assayed the cellular internalization of the Arg4-L and Arg10-L/FITC−BSA or FITC−IgG complexes for a quantitative evaluation of the amount of internalized protein. Cells were exposed to the same conditions as for the flow cytometric analysis and lysed by 0.2% Triton X-100/PBS. FITC−BSA (5 μg/mL) was internalized in the cells at about 40% and 30% of the dose with Arg4-L and with Arg10-L, respectively. On the other hand, FITC−IgG was internalized at about 10% and 19% of the dose with Arg4-L and with Arg10-L, respectively.

Efficiency of the Cellular Uptake of Arg10-L/FITC−IgG Based on the Ratio of Arg10-L to IgG. We examined the optimal molar ratio of Arg10-BDB to IgG in the Arg10-L/FITC−IgG complex, assaying the cellular internalization of various Arg10-L/FITC−IgG complexes by flow cytometry (Figure 5). Here, the molar ratio of Arg10-L/FITC−IgG refers to the ratio of Arg10-BDB to FITC−IgG because the proportion of Arg10-BDB in liposomes was constant (5 mol %). Cells were exposed for 3 h to the Arg10-L/FITC−IgG complex and then trypsinized. The cellular uptake of FITC−IgG increased as the molar ratio of Arg10-L/FITC−IgG increased and seemed to reach a level of saturation above a molar ratio of 100. It could

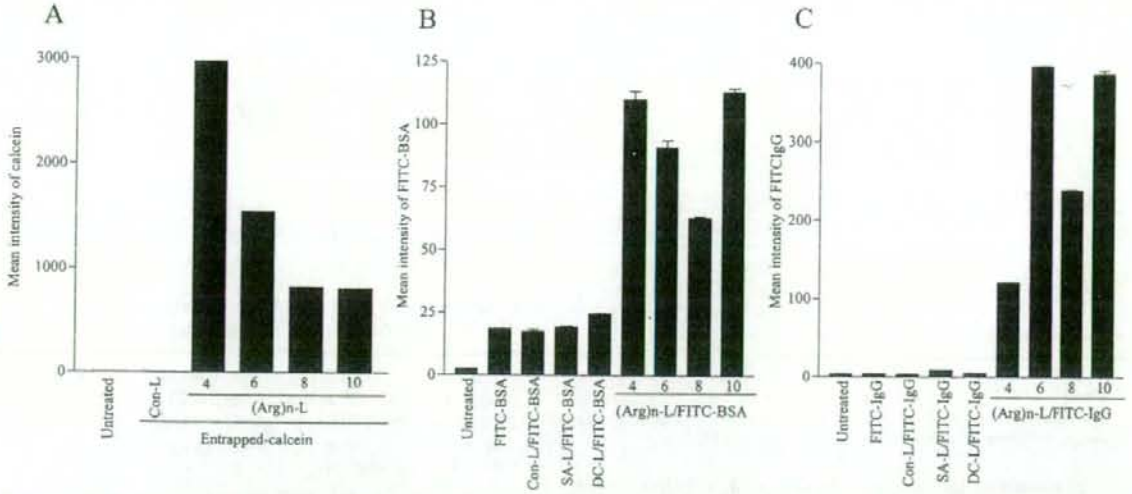

Figure 4. Cellular uptake of the calcein-entrapped $(Arg)_n$-L (A), and $(Arg)_n$-L in complexes with FITC−BSA (B) and FITC−IgG (C). Calcein-entrapped $(Arg)_n$-L (100 μg) alone or each $(Arg)_n$-L/protein complex (a variable $(Arg)_n$-BDB: 5 μg of FITC−BSA or FITC−IgG = 50:1, molar ratio) was diluted with serum-free DMEM to 1 mL and then gently applied to the cells, incubated with the cells for 3 h at 37 °C in serum-free DMEM, and treated with trypsin before FACS analysis. Con-L exhibits liposome without $(Arg)_n$-BDB. SA-L and DC-L exhibit liposome with stearylamine and DC−Chol, respectively. Each value is the mean ± SD of three separate determinations.

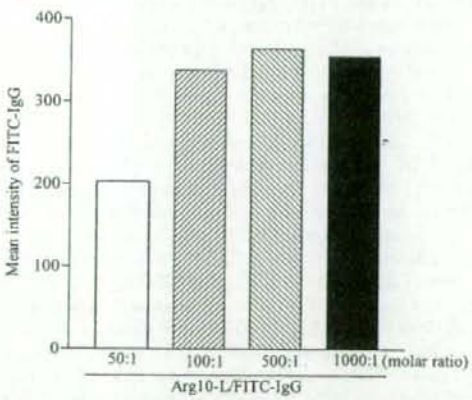

Figure 5. Cellular uptake of the Arg10-L/FITC−IgG complex as a function of the molar ratio between Arg10-BDB and FITC−IgG. Arg10-L/FITC−IgG (a variable Arg10-BDB: 5 μg of FITC−IgG, molar ratio from 50:1 to 1000:1) was diluted with serum-free DMEM to 1 mL and then gently applied to the cells and incubated with the cells at 37 °C for 3 h in serum-free DMEM and treated with trypsin before FACS analysis. Each value is the mean ± SD of three separate determinations.

deliver about 1.5-fold more at a molar ratio of 100 than at 50 without change in the size of the complex.

To confirm the internalization and localization of FITC−IgG in the unfixed cells, we observed the cells by fluorescence microscopy after exposing them to the Arg10-L/FITC−IgG (100: 1) complex for 3 h and washing them five times (Figure 6A, B). FITC−IgG was observed to be taken into almost all cells.

Cellular Uptake of $(Arg)_n$-L/β-Gal Complexes. To examine whether the internalized protein is functional, we observed the enzymatic activity of β-Gal by microscopy. Cells were exposed to the Arg4-L and Arg10-L/β-Gal complexes for 3 h at 37 °C. Then, we observed the efficiency of protein delivery by monitoring the enzymatic activity of β-Gal using X-Gal staining (Figure 7). The cells treated with free β-Gal gave a similar image to untreated cells, suggesting that free β-Gal did not enter the cells (Figure 7A,B). About 70% and 50% of cells with Arg4-L and with Arg10-L, respectively, exhibited strong and uniform

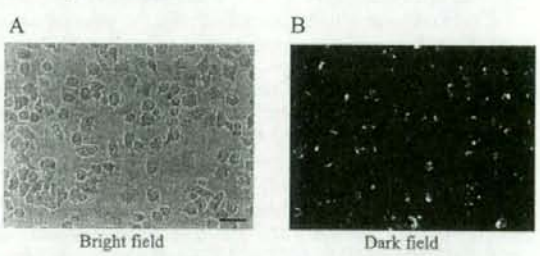

Figure 6. Analysis of FITC−IgG uptake by fluorescence microscopy. Arg10-L/FITC−IgG complex (Arg10:5 μg of FITC−IgG = 100:1, molar ratio) was diluted with serum-free DMEM to 1 mL, gently applied to the cells, and then incubated with the cells for 1 h at 37 °C in serum-free DMEM. The unfixed cells were observed with a fluorescence microscope (magnification × 200). Scale bar = 50 μm.

β-Gal activity (Figure 7C,D). At a higher magnification, we could confirm that β-Gal activity was present in the cytoplasm (Figure 7E,F). The β-Gal activity in the cells treated with Arg4-L and Arg10-L was about 5.9-fold and 4.4-fold stronger, respectively, than that of cells treated with free β-Gal, and β-Gal (5 μg/mL) was internalized in the cells at about 9.7% and 7.2% of the dose with Arg4-L and with Arg10-L, respectively in the chemiluminescence assay. Most notably, the presence of Arg4-L or Arg10-L did not alter the enzymatic activity of β-Gal upon delivery into cells. Arg4-L could deliver β-Gal (120 kDa) more efficiently than Arg10-L, similar to the transport of FITC−BSA. No cytotoxicity was observed for all $(Arg)_n$-L or $(Arg)_n$-L/protein complexes (data not shown).

FIDA Measurements. To examine whether there is a difference in the complex formation, we used FIDA to characterize the interaction of the $(Arg)_n$-L/protein complex. FIDA allows the characterization of fluorescently labeled molecules with respect to their molecular brightness and concentration at the single-molecule level (*18*). Briefly, the FIDA method is based on the collected photon numbers recorded in time intervals of fixed duration (time windows). Using this information, a count number histogram is built up. Then, a theoretical probability distribution of photon numbers is fitted against the obtained histogram, yielding specific brightness values (Q), corresponding to the concentrations (C), for all

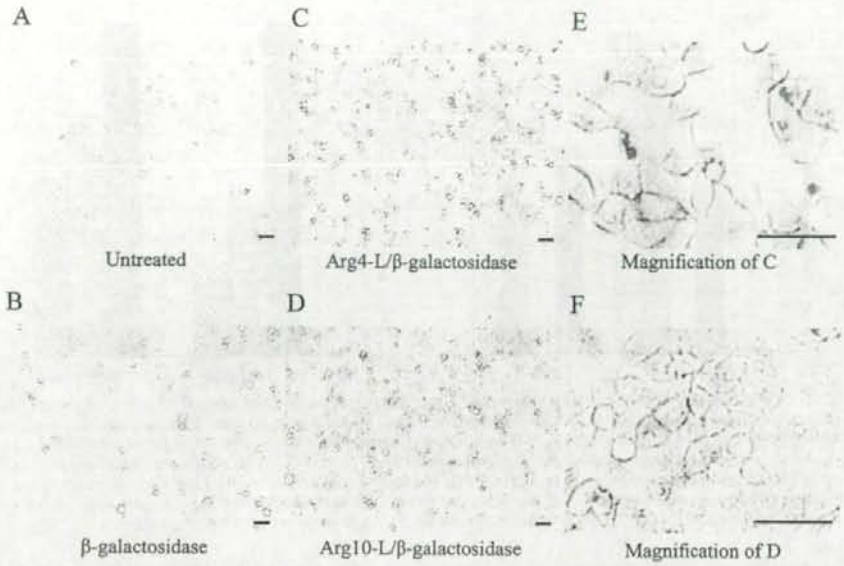

Figure 7. Analysis of β-galactosidase uptake by microscopy. Arg4-L, Arg10-L/β-galactosidase complex (Arg4-BDB or Arg10-BDB: 5 μg of β-galactosidase = 50:1, molar ratio), or 5 μg of β-galactosidase was diluted with serum-free DMEM to 1 mL and then gently applied to the cells and incubated with the cells for 1 h at 37 °C in serum-free DMEM. The cells were stained with a β-galactosidase staining kit and observed with a fluorescence microscope. Scale bar = 50 μm.

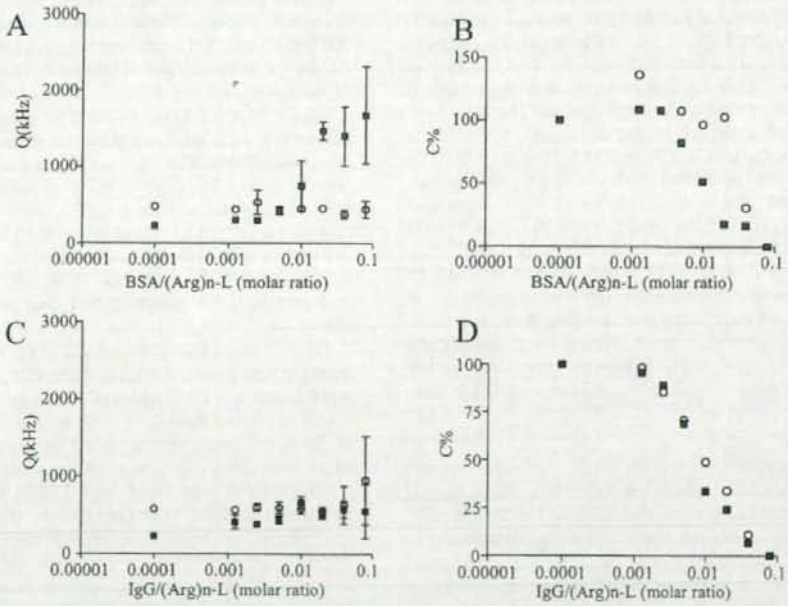

Figure 8. Fluorescence intensity distribution analysis (FIDA) of DiI-labeled Arg4- and Arg10-L/BSA or DiI-labeled Arg4-L and Arg10-L/IgG as a function of the molar ratio between Arg4- or Arg10-BDB and protein. Part A or C was the analytical result of the Q value. Part B or D was the analytical result of the ratio of the C value. Complex was diluted with water. Square, Arg4-L; Circle, Arg10-L. Each value is the mean ± SD of three separate determinations.

different species. To determine the interaction of the $(Arg)_n$-L with proteins, we measured fluorescence intensity distribution of lipid marker, DiI incorporated in the particle lipid layers as a function of the molar ratio between Arg4- or Arg10-L and protein. Here, the molar ratio of the Arg4-L or Arg10-L/protein complex refers to the ratio of Arg4- or Arg10-BDB to protein. Q value of Arg4-L increased at about 0.01 BSA/Arg4-L molar ratio, but that of Arg10-L did not (Figure 8A), corresponding to C value of Arg4-L decreased (Figure 8B). Increase of BSA might form complex with high molar ratio of Arg4-L, which increased brightness per complex (Q value) and decreased fluorescent Arg4-L number (C value). For Arg10-L, the ratio of Arg10-L/BSA in the complex was not changed in this range. Therefore, Q value of the complex was not changed. The interaction of IgG with Arg4-L and Arg10-L was similar (Figure 8C, D).

Mechanism of Cellular Uptake of Arg4-L, Arg10-L, and Complexes. To investigate the internalization mechanism of

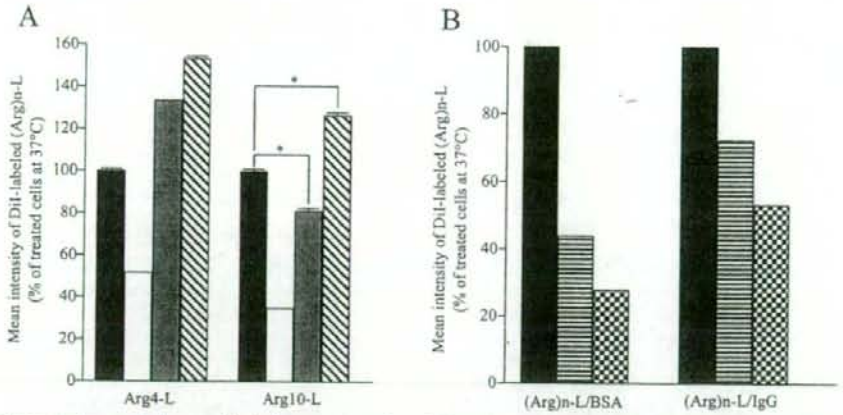

Figure 9. Effect of temperature and pharmacological reagents on the cellular uptake of DiI-labeled $(Arg)_n$-L (A) and $(Arg)_n$-L/protein complex (B). (A) HeLa cells were pretreated with EIPA (25 μM) or PMA (1 μM) at 37 °C for 30 min. The medium was replaced with fresh medium containing DiI-labeled Arg4-L or Arg10-L (100 μg/mL). The cells were incubated for 1 h at 37 °C in serum-free DMEM containing EIPA (25 μM) or PMA (1 μM) and then treated with trypsin before the flow cytometry. Dark bar, 37 °C or no pharmacological reagent; open bar, 4 °C; gray bar, EIPA; slashed bar, PMA. Each value is the mean ± SD of three separate determinations. (B) Effect of temperature on the cellular uptake of DiI-labeled Arg4-L and Arg10-L/protein complex. The experimental conditions were the same as in Figure 4B and C. Dark bar, 37 °C; sideline bar, Arg4-L at 4 °C; mosaic bar, Arg10-L at 4 °C. Each value is the mean ± SD of three independent experiments.

Arg4-L, Arg10-L and their complexes, we prepared DiI-labeled liposomes and examined the effect of temperature, a macropinocytosis inhibitor (EIPA) or an accelerator (PMA) on the cellular uptake of the liposomes. Cells were exposed to DiI-labeled Arg4-L or Arg10-L for 3 h at either 4 °C or 37 °C. Then, they were trypsinized and analyzed by flow cytometry. DiI-labeled Arg4-L and Arg10-L showed about a 50% and 65% lower internalization efficiency, respectively, at 4 °C than at 37 °C (Figure 9A). This finding suggests that the transport occurred through energy-dependent endocytosis. The cells were exposed to DiI-labeled Arg4-L or Arg10-L at 37 °C for 1 h in the absence or presence of EIPA or PMA (Figure 9A). The cellular uptake of Arg4-L increased about 34% in the presence of EIPA, and about 54% in the presence of PMA compared with untreated cells. The cellular uptake of Arg10-L significantly decreased about 20% in the presence of EIPA ($p < 0.05$), but significantly increased about 27% in the presence of PMA ($p < 0.05$) compared with untreated cells. The inhibition of cellular uptake at 4 °C for the Arg4-L/protein complex was lower than that for the Arg10-L/protein complex (Figure 9 B). This finding suggests that Arg4-L and Arg10-L/protein were taken up via an endocytotic pathway as well as Arg4-L or Arg10-L alone.

DISCUSSION

As a free liposome, Arg4-L was most efficiently internalized in the cells. The efficiency decreased depending on the length of oligo-Arg. To our knowledge, this may be the first experimental demonstration that the liposomes with shorter oligo-Arg-L alone were internalized more efficiently than those with longer ones. Besides the demonstration of the free $(Arg)_n$-L cellular uptake, our study reveals protein delivery by $(Arg)_n$-L. Concerning the effect of oligo-Arg length, liposome/protein complexes showed a different trend.

Generally, the cellular uptake of oligo-Arg increases in efficiency as the number of arginine residues increases (*5*). Both Tat and penetratin enhanced the efficiency of the uptake of liposomes in proportion to the number of peptides attached to the liposomal surface (*12*). In our experiments, the shorter oligo-Arg system, Arg4-L, penetrated the cells more efficiently than the longer one, Arg10-L, in the case of calcein-entrapped $(Arg)_n$-L.

To examine the internalization of liposomes, calcein, a water-soluble marker, was entrapped in $(Arg)_n$-L. Liposome−cell interaction on the surface might lead to the leakage of calcein due to liposome destabilization. However, the calcein leakage from $(Arg)_n$-L was small (data not shown). Uptake of DiI-labeled liposomes, which has label-lipid in the liposomes, also exhibited similar behavior to that of calcein-entapped liposomes (data not shown). These findings suggest that the calcein-entrapped $(Arg)_n$-L penetrated as liposomes, and that the difference in the cellular uptake of calcein corresponded to that of the liposomes.

FITC−BSA (66 kDa), β-Gal (120 kDa), and FITC−IgG (150 kDa) were used as model proteins. Cellular uptake of FITC−BSA was increased three to six times when it was in a complex with $(Arg)_n$-L. The highest level of cellular uptake of FITC−BSA was observed with Arg4-L and Arg10-L. For β-Gal, Arg4-L carried β-Gal 6-fold higher than free one. Arg4-L could deliver β-Gal more efficiently than Arg10-L. The enzymatic activity of β-Gal showed a protein to be transported as a biologically active protein. For FITC−IgG, Arg10-L gave the best result.

FIDA showed that the interaction of Arg4-L with BSA was stronger than that of Arg10-L with BSA, and the interaction of Arg4-L and Arg10-L with IgG was similar. At molar ratio of BSA/DiI labeled Arg4-L > 0.02, BSA associated on the surface of liposomes may interact with DiI or the complex may be aggregated. BSA may interact hydrophobic part of Arg4-L. The efficient cellular uptake of Arg4-L/BSA may reflect the strong interaction between Arg4-L and BSA. Also, DiI-labeled Arg4-L in a complex with proteins was taken up more efficiently than Arg10-L complex (data not shown). In the case of IgG, Arg10-L delivered about 3-fold more proteins than Arg4-L (Figure 4C). Because proteins formed complexes with $(Arg)_n$-L prior to the intracellular delivery, it can be postulated that the mode of interactions between proteins and $(Arg)_n$-L might be different depending on the protein.

The cellular uptake was also examined with the fluorescence microscope. To avoid artifacts caused by the fixation procedure, we observed live cells. Fixation was shown to cause significant artifacts regarding the cellular localization (*19*). From the microscopic observation, the fluorescence of FITC−IgG was observed in almost 100% of cells when transported as the Arg10-L complex (Figure 6). From the quantitative evaluation, Arg10-L delivered about 1.2-fold of IgG compared with Arg4-L, whereas FACS analysis indicated that Arg10-L delivered

almost 3-fold more than Arg4-L. The discrepancy could be explained by the sensitivity of fluorescein emission in the microenvironment and partial quenching in the endosomal structures of live cells used for the FACS analysis (*20*).

The cellular translocation by CPP was initially proposed to be an energy-independent process, because no difference was observed in cellular uptake between 37 °C and 4 °C (*2, 5*). However, more recent papers suggest that the majority of the translocation occurs via an energy-dependent pathway, and that the translocation of CPP is reduced by endocytosis inhibitors (*21*−*23*). From the temperature-dependence, the internalization of Arg4-L and Arg10-L was shown to mainly involve endocytosis. Endocytosis represents a variety of mechanisms that fall into two broad categories, phagocytosis and pinocytosis. Phagocytosis is typically restricted to specialized mammalian cells, whereas pinocytosis occurs in most cells via at least four basic mechanisms: macropinocytosis, clathrin-mediated endocytosis, caveolae-mediated endocytosis, and clathrin- and caveolae-independent endocytosis (*24*). In the latest papers, the translocation of Tat peptide is suggested to occur through macropinocytosis which is dependent on lipidic microdomains (*25*), and that of octa-arginine (R8) peptide is also shown to involve macropinocytosis (*26*). EIPA inhibits the Na^+/H^+ exchange and has been shown to inhibit macropinocytosis (*25*). PMA is a protein kinase C activator and stimulates macropinocytosis by increasing membrane ruffles (*27*−*30*). The change in cellular uptake of Arg4-L and Arg10-L caused by a macropinocytosis inhibitor (EIPA) or an accelerator (PMA) suggests that the internalization of Arg10-L occurs mainly through macropinocytosis. Since the cellular translocation of Arg4-L did not decrease by EIPA, it might involve a different mechanism than macropinocytosis.

Pep-1 can efficiently deliver proteins into cells by forming physical assemblies with a variety of proteins at the optimal molar ratio of pep-1 and a protein (*6, 31*). The internalization of pep-1 alone and pep-1/β-Gal complex is not dependent on the endocytotic pathway (*6*). The cellular uptake of the Arg10-L/FITC−IgG complex was greatly enhanced starting from a molar ratio of 50 up to 100 and reached a plateau thereafter. The difference in the behavior of pep-1 and Arg10-L concerning the molar ratio with a protein might also suggest differences in their uptake mechanism.

The most striking result of the present study is that the simple complex formation between oligo-Arg-modified liposomes and proteins, without the entrapment of proteins in the internalized space of liposomes, can produce a cellular transportable protein delivery system, which can deliver active proteins into cells. $(Arg)_n$-L will be useful to deliver macromolecules, which are difficult to entrap in liposomes, into cells. Furthermore, it could release proteins in the cytoplasm because proteins bind on the outer surface of the liposomes. A short oligo-Arg on $(Arg)_n$-L alone may be enough to be taken up in cells, but a longer Arg repeat might be needed to form a complex with large proteins and deliver them into cells. The most suitable (Arg)n-L for a protein delivery could be selected experimentally based on the results of $(Arg)_n$-L complexed with the protein. Such information will be helpful in the design of $(Arg)_n$-L as a carrier for delivering proteins into cells.

In summary, we synthesized $(Arg)_n$-BDB and prepared oligo-Arg modified liposomes as a novel carrier of proteins into cells. We found that the penetrating abilities of $(Arg)_n$-L alone and in complexes with proteins differed. The mechanism of cell membrane penetration of Arg4-L and Arg10-L, and their complexes with proteins, although not thoroughly understood, is probably different.

ACKNOWLEDGMENT

This project was supported in part by a grant from the Promotion and Mutual Aid Corporation for Private Schools of Japan and by a Grant-in-Aid for Scientific Research from the Ministry of Education, Culture, Sports, Science, and Technology of Japan.

LITERATURE CITED

(1) Derossi, D., Joliot, A. H., Chassaing, G., and Prochiantz, A. (1994) The third helix of the Antennapedia homeodomain translocates through biological membranes. *J. Biol. Chem. 269*, 10444−10450.

(2) Vives, E., Brodin, P., and Lebleu, B. (1997) A truncated HIV-1 Tat protein basic domain rapidly translocates through the plasma membrane and accumulates in the cell nucleus. *J. Biol. Chem. 272*, 16010−16017.

(3) Pooga, M., Hallbrink, M., Zorko, M., and Langel, U. (1998) Cell penetration by transportan. *FASEB J. 12*, 67−77.

(4) Oehlke, J., Scheller, A., Wiesner, B., Krause, E., Beyermann, M., Klauschenz, E., Melzig, M., and Bienert, M. (1998) Cellular uptake of an alpha-helical amphipathic model peptide with the potential to deliver polar compounds into the cell interior non-endocytically. *Biochim. Biophys. Acta 1414*, 127−139.

(5) Futaki, S., Suzuki, T., Ohashi, W., Yagami, T., Tanaka, S., Ueda, K., and Sugiura, Y. (2001) Arginine-rich peptides. An abundant source of membrane-permeable peptides having potential as carriers for intracellular protein delivery. *J. Biol. Chem. 276*, 5836−5840.

(6) Morris, M. C., Depollier, J., Mery, J., Heitz, F., and Divita, G. (2001) A peptide carrier for the delivery of biologically active proteins into mammalian cells. *Nat. Biotechnol. 19*, 1173−1176.

(7) Schwarze, S. R., Ho, A., Vocero-Akbani, A., and Dowdy, S. F. (1999) In vivo protein transduction: delivery of a biologically active protein into the mouse. *Science 285*, 1569−1572.

(8) Elliott, G., and O'Hare, P. (1997) Intercellular trafficking and protein delivery by a herpesvirus structural protein. *Cell 88*, 223−233.

(9) Saalik, P., Elmquist, A., Hansen, M., Padari, K., Saar, K., Viht, K., Langel, U., and Pooga, M. (2004) Protein cargo delivery properties of cell-penetrating peptides. A comparative study. *Bioconjugate Chem. 15*, 1246−1253.

(10) Lewin, M., Carlesso, N., Tung, C. H., Tang, X. W., Cory, D., Scadden, D. T., and Weissleder, R. (2000) Tat peptide-derivatized magnetic nanoparticles allow in vivo tracking and recovery of progenitor cells. *Nat. Biotechnol. 18*, 410−414.

(11) Torchilin, V. P., Rammohan, R., Weissig, V., and Levchenko, T. S. (2001) TAT peptide on the surface of liposomes affords their efficient intracellular delivery even at low temperature and in the presence of metabolic inhibitors. *Proc. Natl. Acad. Sci. U.S.A. 98*, 8786−8791.

(12) Tseng, Y. L., Liu, J. J., and Hong, R. L. (2002) Translocation of liposomes into cancer cells by cell-penetrating peptides penetratin and tat: a kinetic and efficacy study. *Mol. Pharmacol. 62*, 864−872.

(13) Mitchell, D. J., Kim, D. T., Steinman, L., Fathman, C. G., and Rothbard, J. B. (2000) Polyarginine enters cells more efficiently than other polycationic homopolymers. *J. Pept. Res. 56*, 318−325.

(14) Wender, P. A., Mitchell, D. J., Pattabiraman, K., Pelkey, E. T., Steinman, L., and Rothbard, J. B. (2000) The design, synthesis, and evaluation of molecules that enable or enhance cellular uptake: peptoid molecular transporters. *Proc. Natl. Acad. Sci. U.S.A. 97*, 13003−13008.

(15) Futaki, S., Ohashi, W., Suzuki, T., Niwa, M., Tanaka, S., Ueda, K., Harashima, H., and Sugiura, Y. (2001) Stearylated arginine-rich peptides: a new class of transfection systems. *Bioconjugate Chem. 12*, 1005−1011.

(16) Hara, M., Takanashi, Y., Tuzuki, N., Kawakami, H., Toma, K., and Higuchi, A. (2003) Production of interferon-β by NB1−RGB cells cultured on peptide-lipid membranes. *Cytotechnology 42*, 13−20.

(17) Furuhata, M., Kawakami, H., Toma, K., Hattori, Y., and Maitani, Y. (2006) Design, synthesis and gene delivery efficiency of novel oligo-arginine-linked PEG-lipids: Effect of oligo-arginine length. *Int. J. Pharm. 316*, 109−116.

(18) Kask, P., Palo, K., Ullmann, D., and Gall, K. (1999) Fluorescence-intensity distribution analysis and its application in biomolecular detection technology. *Proc. Natl. Acad. Sci. U.S.A. 96*, 13756−13761.

(19) Richard, J. P., Melikov, K., Vives, E., Ramos, C., Verbeure, B., Gait, M. J., Chernomordik, L. V., and Lebleu, B. (2003) Cell-penetrating peptides. A reevaluation of the mechanism of cellular uptake. *J. Biol. Chem. 278*, 585−590.

(20) Fischer, R., Kohler, K., Fotin-Mleczek, M., and Brock, R. (2004) A stepwise dissection of the intracellular fate of cationic cell-penetrating peptides. *J. Biol. Chem. 279*, 12625−12635.

(21) Vives, E. (2003) Cellular uptake of the Tat peptide: an endocytosis mechanism following ionic interactions. *J. Mol. Recognit. 16*, 265−271.

(22) Drin, G., Cottin, S., Blanc, E., Rees, A. R., and Temsamani, J. (2003) Studies on the internalization mechanism of cationic cell-penetrating peptides. *J. Biol. Chem. 278*, 31192−31201.

(23) Fischer, R., Waizenegger, T., Kohler, K., and Brock, R. (2002) A quantitative validation of fluorophore-labelled cell-permeable peptide conjugates: fluorophore and cargo dependence of import. *Biochim. Biophys. Acta 1564*, 365−374.

(24) Conner, S. D., and Schmid, S. L. (2003) Regulated portals of entry into the cell. *Nature 422*, 37−44.

(25) Wadia, J. S., Stan, R. V., and Dowdy, S. F. (2004) Transducible TAT-HA fusogenic peptide enhances escape of TAT-fusion proteins after lipid raft macropinocytosis. *Nat. Med. 10*, 310−315.

(26) Nakase, I., Niwa, M., Takeuchi, T., Sonomura, K., Kawabata, N., Koike, Y., Takehashi, M., Tanaka, S., Ueda, K., Simpson, J. C., Jones, A. T., Sugiura, Y., and Futaki, S. (2004) Cellular uptake of arginine-rich peptides: roles for macropinocytosis and actin rearrangement. *Mol. Ther. 10*, 1011−1022.

(27) Holm, P. K., Eker, P., Sandvig, K., and van Deurs, B. (1995) Phorbol myristate acetate selectively stimulates apical endocytosis via protein kinase C in polarized MDCK cells. *Exp. Cell Res. 217*, 157−168.

(28) Amyere, M., Payrastre, B., Krause, U., Van Der Smissen, P., Veithen, A., and Courtoy, P. J. (2000) Constitutive macropinocytosis in oncogene-transformed fibroblasts depends on sequential permanent activation of phosphoinositide 3-kinase and phospholipase C. *Mol. Biol. Cell. 11*, 3453−3467.

(29) Riezman, H., Woodman, P. G., van Meer, G., and Marsh, M. (1997) Molecular mechanisms of endocytosis. *Cell 91*, 731−738.

(30) Grimmer, S., van Deurs, B., and Sandvig, K. (2002) Membrane ruffling and macropinocytosis in A431 cells require cholesterol. *J. Cell Sci. 115*, 2953−2962.

(31) Henriques, S. T., Costa, J., and Castanho, M. A. (2005) Translocation of beta-Galactosidase Mediated by the Cell-Penetrating Peptide Pep-1 into Lipid Vesicles and Human HeLa Cells Is Driven by Membrane Electrostatic Potential. *Biochemistry 44*, 10189−10198.

BC060034H

Available online at www.sciencedirect.com
SCIENCE DIRECT
Journal of Controlled Release 113 (2006) 146–154
journal of controlled release
www.elsevier.com/locate/jconrel

Novel ultra-deformable vesicles entrapped with bleomycin and enhanced to penetrate rat skin

Yuka Hiruta [a], Yoshiyuki Hattori [a], Kumi Kawano [a], Yasuko Obata [b], Yoshie Maitani [a,*]

[a] Institute of Medicinal Chemistry, Hoshi University, Ebara 2-4-41, Shinagawa-ku, Tokyo 142-8501, Japan
[b] Department of Pharmaceutics, Hoshi University, Ebara 2-4-41, Shinagawa-ku, Tokyo 142-8501, Japan

Received 18 January 2006; accepted 30 April 2006

Abstract

Beta-sitosterol 3-β-D-glucoside (Sit-G), an absorption enhancer, was incorporated into ultra-deformable vesicles containing bleomycin to attenuate drug toxicity in human keratinocytes. The presence of Sit-G increased drug entrapment and improved in vitro stability of ultra-deformable vesicles. Confocal laser scanning microscopy revealed the extent to which Sit-G facilitated the penetration of ultra-deformable vesicles containing fluorescent probes into rat skin upon non-occlusive topical application. Furthermore, treatment with preparations incorporating Sit-G resulted in elevated epidermal and dermal concentrations of bleomycin. Ultra-deformable formulation contained Sit-G maintained flexibility for penetration through the skin, increased entrapment efficiency of bleomycin and stability in vitro, and significantly increased distribution of bleomycin in epidermis and dermis compared with those without Sit-G.

Keywords: Ultra-deformable vesicle; Bleomycin; Skin permeation; Sodium cholate; Sterylglucoside

1. Introduction

The surface of human skin consists of the epidermis and stratum corneum (SC) layers. Despite their natural barrier properties, several drugs have successfully been delivered through these layers and the use of transdermal drug delivery systems have recently increased in popularity. In order to cross intact skin, drug carriers must either pass through corneocytes, or in between them via intercellular spaces. Many approaches have been developed to either destroy or fluidize the lipid bilayers, thereby, enhancing the penetration of drugs [1]. The diffusivity and solubility of the drug carrier in the SC and epidermis are critical parameters, which control the rate of drug permeation in skin [2].

Lipid vesicles drug delivery systems can be biocompatible in humans and incorporate both hydrophilic and lipophilic drugs [3]. Edge activators can increase the elasticity of bilayers formed from the redistribution of amphiphilic lipids [4] and such ultra-deformable vesicles have been shown to penetrate intact skin via transdermal osmotic gradients and hydration forces [5]. Examples of edge activators include the surfactants: sodium cholate, sodium deoxycholate [6,7], Tween 80 and Span 80 [8].

Bleomycin is an established anti-tumour drug used in the treatment of non-melanoma skin cancer (NMSC). Recent work has shown that bleomycin can be encapsulated in ultra-deformable liposomes [9] and this preparation may be useful for topical chemotherapy of NMSC [10].

Beta-sitosterol 3-β-D-glucoside (Sit-G, Fig. 1) exhibits slight solubility in water and oil. Particulate Sit-G exhibited the novel capability of promoting transport of peptide drugs through the intestinal and nasal mucosae by being ascribed to the glucose residue [11,12]. Sit-G was expected to be an absorption enhancer for skin.

The purpose of this investigation is to study the physical properties of ultra-deformable liposomes incorporating Sit-G.

* Corresponding author. Tel./fax: +81 3 5498 5048.
E-mail address: yoshie@hoshi.ac.jp (Y. Maitani).

0168-3659/$ - see front matter © 2006 Elsevier B.V. All rights reserved.
doi:10.1016/j.jconrel.2006.04.016

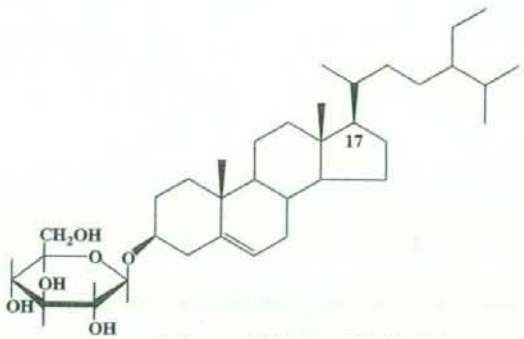

ß-sitosterol ß-D-glucoside (Sit-G)
MW; 580.60

Fig. 1. Chemical structure of β-sitosterol β-D-glucoside (Sit-G).

In order to enhance permeation of drugs through skin, we developed a novel formulation of ultra-deformable vesicles incorporating an absorption enhancer, Sit-G.

2. Materials and methods

2.1. Materials

Bleomycin hydrochloride for injection (BLM) was a gift from Nippon Kayaku Co. (Tokyo, Japan). Egg phosphatidylcholine (EPC) was purchased from NOF Corp. (Tokyo, Japan). Sit-G was obtained from Essential Sterolin Products (Midrand, South Africa). Tween 80 (Tween) and calcein were purchased from Tokyo Kasei Kogyo Co. Ltd. (Tokyo, Japan). Sodium cholate (Cholate), sodium perchlorate and urethane were obtained from Sigma Chemicals Co. (St. Louis, MO, U.S.A.). 1,1′-Dioctadecyl-3,3,3′,3′-tetramethylindocarbocyanine perchlorate (DiI) was purchased from Lambda Probes and Diagnostics (Graz, Austria). Other chemicals used were of reagent grade and purchased from Wako Pure Chemical Industries Ltd. (Osaka, Japan).

2.2. Preparation of ultra-deformable vesicles entrapped with calcein or BLM

Ultra-deformable vesicles were prepared by a dry film method. Briefly, lipid mixtures of EPC, Tween or Cholate, were dissolved in ethanol. Sit-G was dissolved in a chloroform/methanol solvent system at 2:1 v/v ratio. Then these lipid solutions were mixed. This organic solvent system was removed by rotary evaporation, under vacuum and at 55 °C. The dry lipid film was hydrated with either Milli-Q water, 1 mg/mL BLM aqueous solution, or 20 mM calcein solution, to yield empty vesicles, BLM-entrapped vesicles (BLM-vesicles), or calcein-entrapped vesicles, respectively. Vesicles labelled with DiI were prepared by addition of DiI (0.4 mol%) to lipid mixtures and hydrating with Milli-Q water. Vesicles were subsequently sonicated for 2–10 min using a bath-type sonicator (UT-205S, Sharp Corp., Osaka, Japan) at a 200 W energy output. Final total lipid concentration in all formulations was 10 mg/mL.

2.3. Vesicle size, morphology and ζ-potential measurements

Average diameters and ζ-potentials of vesicles were measured by dynamic light-scattering (DLS) and electrophoresis light-scattering methods, respectively (ELS 800, Otsuka Electronics, Osaka, Japan). All measurements were performed at 25±1 °C, after diluting the vesicle suspension with Milli-Q water.

Particle morphology was analyzed using a scanning electron microscope (SEM, JSM-5600LV, JEOL Ltd., Tokyo, Japan). Samples were coated with platinum prior to analysis. An accelerating potential of 15 keV was used and the images were obtained with a scintillating secondary electron detector.

2.4. Measurement of elasticity value

The elasticity value of bilayer of ultra-deformable vesicles was directly proportional to $J_{\text{flux}} \times (r_v/r_p)^2$;

$$\text{Elasticity} = J_{\text{flux}} \times (r_v/r_p)^2$$

where J_{flux} is the rate of penetration through a permeability barrier, r_v is the size of vesicles after extrusion and r_p is the pore size of the barrier [13,14]. To measure J, the vesicles were extruded through a polycarbonate membrane (Nuclepore, Whatman Inc., MA, USA) with a pore diameter of 50 nm (r_p), at a pressure of 0.5 MPa. After 5 min of extrusion, the extrudate was weighed (J), and the average vesicle diameter after extrusion (r_v) was measured by DLS.

2.5. Captured volume of ultra-deformable vesicles

Calcein-entrapped vesicles were separated from free (unentrapped) calcein by gel filtration chromatography using a Sephadex G-50 column and a mobile phase of 1/10 diluted phosphate-buffered saline (1/10 PBS). Vesicles were disrupted by addition of 10% (v/v) Triton X-100 (final concentration 0.1%) to release their calcein load. Entrapment efficiency was calculated by measurement of fluorescence emitted from entrapped calcein, and by EPC quantification via enzyme assay (Phospholipid B Test Wako, Wako Pure Chemical Industries Ltd.). Captured volume was obtained from calculated values of calcein entrapment efficiency and total post-filtration lipid concentration [15].

2.6. Determination of BLM-entrapment efficiency

Free BLM was separated from entrapped BLM using a Sephadex G-50 column and a mobile phase of 1/10 PBS. Unentrapped BLM was quantified by a UV-spectrophotometer (UV-1700 Phamaspec, Shimadzu Corp., Kyoto Japan) at 292 nm. Entrapment efficiency of BLM was calculated

indirectly from the amount of free drug, according to the following equation:

$$\text{Entrapment efficiency } (\%) = (1 - B_f/B_t) \times 100$$

where B_f was the amount of free BLM and B_t was the total amount of BLM.

2.7. Physical stability study of BLM-vesicles in vitro

The stability of BLM-vesicles (10 mg/mL total lipid concentration) was evaluated by monitoring entrapment efficiency of BLM for 1 h at 37 °C [8]. Samples of the original vesicle suspensions, unfiltered and undiluted, were incubated at 37 °C. After 1 h, 100 μL aliquots were taken for determination of entrapment efficiency using the method in Section 2.6. Entrapment efficiency was calculated indirectly from the percentage of drug released. The amount entrapped at start time was normalized to 100%.

2.8. Animals

Wistar rats (male, 7 weeks, 190–220 g) and hairless rats (male, 7 weeks, 190–210 g) with clean status were purchased from Tokyo Laboratory Animal Science Co., Ltd. (Tokyo, Japan) and Sankyo Labo Service Corp. (Tokyo, Japan), respectively. They were housed in animal facilities under standard laboratory conditions prior to experimentation.

2.9. In vivo skin deposition and partitioning of BLM

Prior to experimentation, hair was carefully removed with an electric clipper from the abdominal area of Wistar rats under anesthesia (intra-peritoneal injection of urethane, 1 g/kg). Cevc and Blume [5] had previously recommended non-occlusive application for optimum transdermal drug delivery with ultra-deformable vesicles. The individual BLM-vesicle suspension containing 157 μg of liposomal BLM without gel filtration and the BLM solution (157 μg BLM using 1 mg/mL) were non-occlusively applied on the abdomen of rats (3.14 cm^2) for either 3 or 12 h. Rats were kept on their back on a heating pad during the sedation period. Blood sample (1 mL) was collected from the jugular vein periodically for either 3 or 12 h after dosing, and then centrifuged at 13,000 rpm for 4 min to obtain serum. After percutaneous administration of suspension, the residual suspension was removed from the skin surface with a cotton swab with warm water. The full-thickness skin was then separated from the underlying tissue. The serum and full-thickness skin was stored at −20 °C until HPLC analysis.

For in vivo skin partitioning of BLM after 12 h application, the BLM-vesicle suspensions remaining on the skin surface were wiped off with warm water. Stratum corneum (SC) was obtained using tape-strip technique. Ten strips and stripped skin (viable epidermis plus dermis) were further processed for HPLC analysis.

2.10. Sample preparation and HPLC assay

The serum (400 μL) was also centrifuged at 13,000 rpm for 4 min following to addition of 20% (w/v) trichloroacetic acid (TCA, 100 μL). The full-thickness and stripped skin were cut into small pieces and homogenized in 2 mL of 10 mM sodium perchlorate in 0.1% aqueous phosphoric acid (solvent A). After addition of 1 mL of 20% (w/v) TCA, the homogenate was centrifuged at 15,000 rpm for 5 min. The supernatants of serum and sample (300 μL) were directly injected into the HPLC system to determine the concentration of BLM. The recovery of added amounts of BLM to serum and skin homogenate was 89.6 ±9.6% and 87.9±16.7%, respectively. The SC tape-strips were soaked in 5 mL of solvent A for 5 h at room temperature. After removal of the tapes, SC sample was freeze-dried and dissolved in 800 μL of solvent A.

The HPLC analysis was performed at 25 °C. The system was consisted of SCL-10A system controller, LC-10AT liquid chromatograph, SIL-10AF auto injector, SPD-10A UV spectrophotometric detector at 240 nm (Shimadzu Corp.), and a C_{18} column (YMC-Pack, ODS-A A-302, 150×4.6 mm I.D., YMC Co., Ltd., Japan). The mobile phase was consisted of solvent A and acetonitrile (solvent B). A line gradient was applied from 5% to 25% solvent B for 20 min, increasing within 2 min to 100% B and hold for a 2 min and followed by post-time of 8 min under the initial condition [16]. The flow rate was set at 1 mL/min.

2.11. In vivo distribution of fluorescent-labeled ultra-deformable vesicles

Vesicle contained 16% (w/w) Cholate and 5% (w/w) Sit-G (CS-vesicles) suspension labeled by both DiI and calcein (551 μL; containing 14.8 mM of total lipid, 59 μM DiI and 20 mM calcein) without gel filtration, the mixture suspension of 20 mM calcein and DiI-labeled CS16-vesicles (Table 1) (551 μL; containing 14.8 mM of total lipid and 59 μM DiI) and the mixture solution (551 μL) of 20 mM calcein and 59 μM DiI were applied on the abdominal skins of hairless rats for 3 h

Table 1
The formulation of ultra-deformable vesicles

Vesicles	EPC	Tween 80 (T)	Sodium cholate (C)	Sit-G (S)
			% (w/w)	
EPC	100	–	–	–
T6	94	6	–	–
10	90	10	–	–
16	84	16	–	–
26	74	26	–	–
C6	94	–	6	–
10	90	–	10	–
16	84	–	16	–
26	74	–	26	–
CS6	89	–	6	5
10	85	–	10	5
16	79	–	16	5
26	69	–	26	5

T-, C- and CS-vesicle were composed of Tween 80, sodium cholate, and sodium cholate and Sit-G, respectively.

under anesthesia. After the removal of excess suspension, the skins administered were excised, washed three times with Milli-Q water and then dried with cotton swab. The skins were embedded in OCT compound (Tissue-Tek, Sakura Finetechnical Co., Ltd., Tokyo, Japan) and processed for frozen sectioning. The embedded skins were sectioned; frozen sections 20 μm apart of both cut surfaces. Each frozen section was mounted on a MAS coat slide glass (SUPERFROST®, Matsunami, Osaka, Japan), and examined microscopically. A confocal laser-scanning microscope (CLSM, Radiance 2100, Bio-Rad Laboratories, Inc., Hercules, CA, U.S.A.) was employed for imaging. For DiI, maximum excitation was performed by a 543-nm line of internal He–Neon laser, and fluorescence emission was observed with long pass barrier filter 560DCLP. Calcein was imaged using the 488 nm excitation line of an argon laser, and fluorescence emission was observed with a filter HQ515/30. The contrast level and brightness of the images were adjusted.

2.12. Statistical analysis

Significant differences in the mean values were evaluated by the Student's unpaired *t*-test. A *p*-value of less than 0.05 was considered to be significant.

3. Results

3.1. Elasticity of vesicles

Elasticity is an important feature of ultra-deformable vesicles that differentiates it from other lipid disperse systems which are typically non-elastic. Four formulations were used (Table 1): control vesicles containing only EPC (EPC-vesicles), EPC-vesicles containing a surfactant (Tween or Cholate, T- or C-vesicles), and C-vesicles incorporating 5% (w/w) Sit-G (CS-vesicles).

Average vesicle diameters of each preparation, before and after extrusion, are shown in Table 2. Preparations containing 26% (w/w) Cholate, either with (CS26) or without (C26)

Table 2
Size of empty ultra-deformable vesicles before and after extrusion through polycarbonate membrane with a pore size of 50 nm

Vesicles	Size before extrusion (nm)	Size after extrusion (nm)
EPC	155.4±9.2	80.3±9.0
T6	150.7±13.3	102.7±17.2
10	139.6±5.3	114.7±1.0
16	136.7±7.8	102.3±10.4
26	125.4±7.9	112.6±12.8
C6	156.3±9.2	122.7±3.7
10	143.3±3.3	122.9±0.7
16	140.0±5.2	108.4±2.5
26	66.6±15.4	48.6±9.9
CS6	143.0±8.9	114.7±1.1
10	140.0±4.1	112.5±2.9
16	148.0±1.0	110.5±0.8
26	66.1±23.1	52.8±17.4

Values represented as mean±S.D.(n=3).

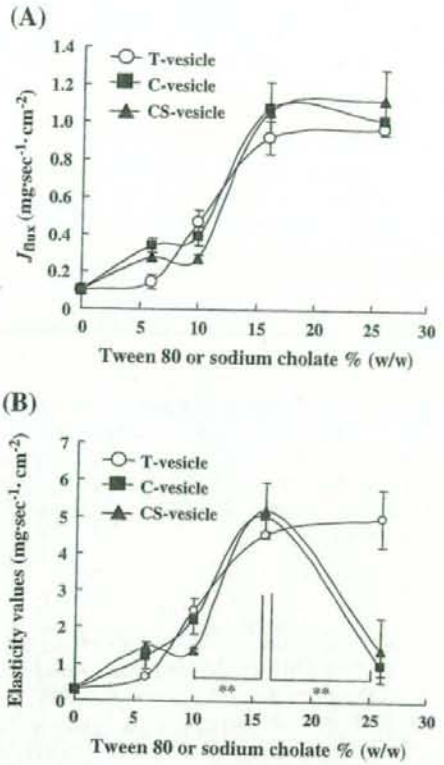

Fig. 2. J_{flux} (A) and calculated elasticity values, $J_{flux} \times (r_v/r_p)^2$ (B) of empty ultra-deformable vesicles in relation to the content of Tween 80 or sodium cholate. Each value represents the mean±S.D. (n=3). **p<0.01.

5% (w/w) Sit-G, exhibited average vesicle diameters of 66 nm. Average vesicle diameters of all other preparations were in the range of 125–155 nm. Over the course of 5 months storage at room temperature, significant changes in vesicle size were only observed in the control preparation (data not shown). A reduction in average vesicle diameter was observed in all preparations after extrusion. Except for C26, CS26 and control formulations, the average vesicle diameter of ultra-deformable vesicles remained above 100 nm after extrusion (Table 2).

J_{flux} started at 16% (w/w) surfactant concentration in T-, C- and CS-vesicles (Fig. 2A) and elasticity of C- and CS-vesicles peaked to plateau at this concentration (Fig. 2B). At the highest concentrations of surfactant, reductions of vesicle size and elasticity were observed in C26 and CS26 (Table 2 and Fig. 2B), whereas no reduction of them was observed in T26. Elasticity of the preparations (T- or C-vesicles) in this investigation was comparable with published data [8].

The recovery of vesicle suspensions after extrusion was determined by measuring EPC concentrations in the extrudate when the passage of vesicles through pores much smaller than their own diameter (Fig. 3). The recovery of EPC of EPC-vesicle was approximately 10%. That in T-, C- and CS-vesicles was increased with an increase of surfactant

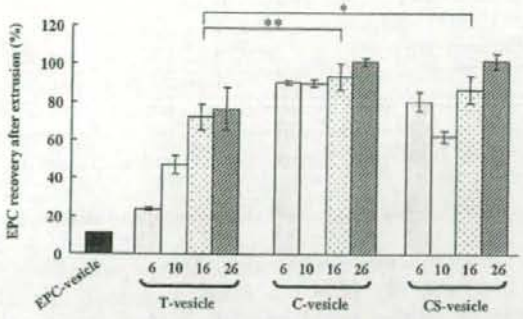

Fig. 3. EPC recovery (%) in vesicle suspensions after extrusion through polycarbonate membrane with a pore size of 50 nm. Each value represents the mean±S.D. (n=3). *p<0.05, **p<0.01.

content in each formulation. C16- and CS16-vesicles with maximum elasticity passed through the polycarbonate membrane showed about 80% of EPC, which was significantly higher compared with that of T-vesicles (p<0.05). C26- and CS26-vesicles showed high EPC recovery because of small sizes.

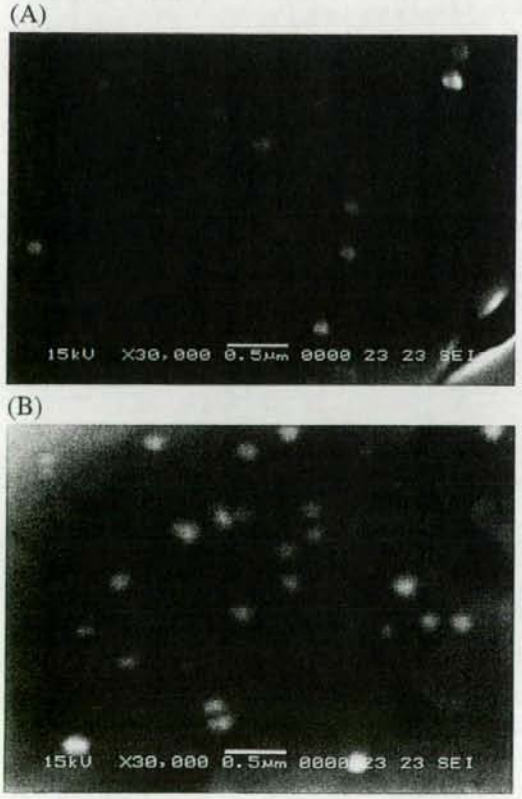

Fig. 4. Scanning electron micrographs of C16-vesicles before (A) and after extrusion (B) through a polycarbonate membrane with a pore size of 50 nm. Scale bar=0.5 μm.

The morphology of vesicles was also investigated by scanning electron microscopy. C16-vesicles were chosen for SEM observation because of their high elasticity and EPC recovery. C16-vesicles after extrusion appeared as particles with a diameter of above 100 nm, like vesicles before extrusion (Fig. 4A, B). High recovery of EPC and SEM observation of vesicle suspensions after extrusion suggest that high elasticity of the bilayers, ultra-deformable vesicles might squeeze themselves and pass through pores much smaller than their own diameter.

3.2. Captured volume and ζ-potential of empty vesicles and characterization of BLM-entrapped vesicles

Based on the result of extrusion measurement, highly elastic T16-, C16- and CS16-vesicles were chosen as the formulations of BLM-vesicles (T16-, C16- and CS16-BLM, respectively) for stability study. The volume of entrapped aqueous fluid per mole of lipid represented the captured volume afforded by the preparation, and this parameter has been linked with many membrane properties [17,18]. In this experiment, captured volume was calculated from the entrapment efficiency of calcein. Captured volume of the T16-, C16- and CS16-vesicles was 1.7±0.06 μL/μmol, 1.4± 0.11 μL/μmol and 1.0±0.03 μL/μmol, respectively (Table 3). This finding suggests that the inner aqueous phase of vesicles was significantly decreased with the increase of other components into EPC.

C16- and CS16-vesicles were more negatively-charged than T16-vesicles (Table 3). Vesicles containing Cholate showed particularly negative ζ-potentials, but CS16-vesicles showed less negative ζ-potential than C16-vesicles, suggesting that Sit-G might disturb the charge of Cholate at the surface of vesicles. The entrapment efficiencies of BLM-vesicles are given in Table 3. The average size of BLM-vesicles was about 145–158 nm. Of the formulations, higher efficiency of BLM was as follows; CS16-BLM>C16-BLM>T16-BLM≈EPC-BLM, and CS16-BLM gave the highest entrapment efficiency; 28.5%. C16 was more negative than CS16, but had lower efficiency. This finding suggests that positively-charged BLM might lead to the

Table 3
Characteristics of empty and BLM-vesicles

Vesicles	Empty vesicles		BLM-vesicles[a]
	Captured volume[b] (μl/μmol)	ζ-potential (mV)	Entrapment efficiency (%)
EPC			10.4±0.8
T16	1.7±0.06	−3.48	13.2±2.1
C16	1.4±0.11	−37.6	22.7±1.1
CS16	1.0±0.03	−30.7	28.5±1.7

Each value represents the mean±S.D.(n=3) except ζ-potential (n=2). *p<0.05.
[a]Average size of BLM-vesicles was 145–158 nm.
[b]Ratio of captured volume (μL) over mole (μmol) of lipids. Captures volume was calculated from entrapment efficiency of calcein.

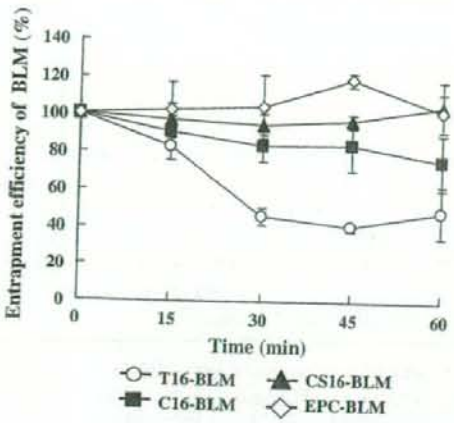

Fig. 5. Stability of BLM-vesicles by monitoring entrapment efficiency. BLM-vesicles prepared using 1 mg/mL BLM aqueous solution without gel filtration were incubated at 37 °C. Each value represents the mean±S.D. (n=3). Total lipid concentration of each vesicle was 10 mg/mL.

binding with Cholate and also interact with Sit-G molecules incorporated into the membrane.

Fig. 5 illustrates the result of the stability of BLM-vesicles without gel filtration, assuming the entrapped amount to be 100% before incubation. Entrapment efficiency of CS16-, C16- and EPC-BLM preparations after 1 h of incubation at 37 °C was approximately 105%, 80%, and 102%, respectively. Preparations made from CS16-BLM were very stable and similar to EPC-BLM, whereas T16-BLM showed rapid release of BLM such that over 50% of entrapped BLM was lost within the initial 30 min (Fig. 5). These differences might be due to variations in molecular ordering caused by using particular surfactants. Preparations made from CS16-BLM were stable and showed high BLM entrapment efficiency, suggesting strong interaction between BLM and the Sit-G incorporated in vesicle bilayers. After gel filtration, the entrapment efficiency of CS16-, C16- and EPC-BLM preparations were less than that without gel filtration after 1 h incubation at 37 °C (data not shown). This finding suggests that BLM was highly released from CS16-, C16- and EPC-BLM preparations after gel filtration at 37 °C. Consequently, in the following in vivo permeation studies, BLM-vesicles were used without gel filtration.

3.3. In vivo skin permeation and deposition of BLM

Skin permeation of BLM arising from preparations of C16-, CS16-, and EPC-BLM was examined in vivo. Free BLM aqueous solution (BLM sol.) was used as a control. The permeation profile of BLM as a function of time is presented in Fig. 6. The skin permeation of C16-, CS16-, and EPC-BLM showed 1.8±0.5, 3.1±0.4 and 0.8±0.2 dose% at 3 h and 4.0±1.0, 6.0±1.2 and 1.1±0.4 dose% at 12 h, respectively.

Skin permeation and deposition of BLM sol. showed no detectable levels of BLM, either in serum or in full-thickness skin (skin; <0.5 dose%, serum; <2.9 dose%). This indicated that free BLM did not permeate into the rat skin over a period of 12 h. The absorption of BLM into the skin from vesicle formulations was observed but serum concentrations of BLM were not detectable. Preparations of CS16-BLM showed significantly higher concentrations of BLM than EPC-BLM, at both 3 and 12 h (p<0.01).

Distribution of BLM in skin 12 h after application (Fig. 7) revealed that EPC-BLM preparations only showed detectable levels of BLM in SC and not beyond. By comparison, C16- and CS16-BLM showed preferential absorption of BLM into epidermis and dermis rather than merely residing in the SC. Preparations of CS16-BLM delivered higher skin concentrations of BLM than C16-BLM (p<0.01), and BLM levels in epidermis plus dermis were approximately twice as high as that

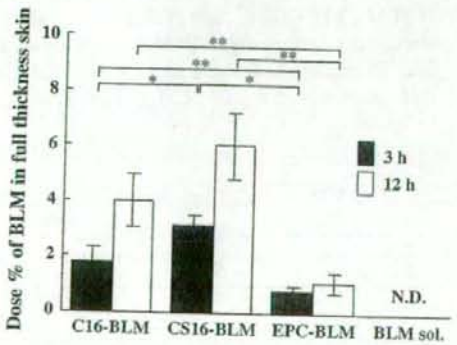

Fig. 6. Deposition of BLM in full-thickness skin 3 h and 12 h after application of ultra-deformable vesicles on Wistar rat. BLM-vesicles contained 157 μg of BLM as an entrapped amount without gel filtration, and the BLM solution (157 μg BLM using 1 mg/mL) were non-occlusively applied on the abdomen of rats (3.14 cm^2). N.D.; not detected. Each value represents the mean±S.D. (n=3), * p<0.05, ** p<0.01.

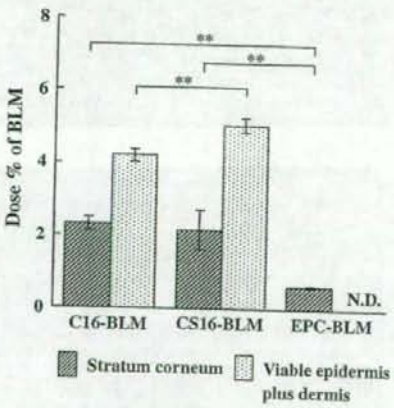

Fig. 7. Distribution of BLM in different layers of the skin of Wistar rat 12 h after non-occlusive application of vesicles. Vesicles contained 157 μg of BLM as an entrapped amount without gel filtration. Stratum corneum and viable epidermis plus dermis were obtained from the treated full-thickness skin. N.D.; not detected in viable epidermis plus dermis. Each value represents the mean±S.D. (n=3), ** p<0.01.

in the SC. These findings suggest that CS16 was more effective as a carrier for delivering BLM topically into the skin than C16 vesicles.

3.4. Permeation of CS16-vesicle through the skin observed by CLSM

The ability of CS16-vesicles to deliver encapsulated hydrophilic fluorescent probes into full-thickness skin was observed by CLSM. Sections of hairless rat skin were treated for 3 h with a topical preparation of CS16-vesicles labelled with DiI and entrapped with calcein (Fig. 8A); a mixture suspension of free calcein and DiI-labeled empty CS16-vesicles (Fig. 8B); and a mixture solution of free DiI and calcein as a control (Fig. 8C). When CS16-vesicles labelled with DiI and containing calcein were applied, the fluorescence of calcein appeared to be quite uniform and quite intense in the whole SC. Co-location of calcein and DiI, which produced a yellow colour, was observed extensively, even in the bottom of SC (Fig. 8A). However, a mixture of calcein and empty CS16-vesicles delivered less intense fluorescence when compared against the first formulation (Fig. 8A vs. B). Finally, from the mixture solution of free DiI and calcein, it could be clearly seen that fluorescence of lipophilic DiI was homogenously distributed across the SC and free calcein was unable to penetrate into the SC (Fig. 8C). This finding suggests that ultra-deformable vesicles could deliver hydrophilic drugs encapsulated in vesicles.

4. Discussion

We have already reported that BLM can be encapsulated in ultra-deformable vesicles composed of EPC and Cholate for topical application [10]. To enhance permeation of drug through skin, we developed a novel, ultra-deformable vesicle incorporating Sit-G, an effective absorption enhancer in intestinal and nasal mucosae [11,12].

In this study we report the efficacy of ultra-deformable formulations containing Sit-G and loaded with the candidate drug BLM. Penetration of lipid vesicles through skin is related to the deformability of the vesicle membrane and only optimized carriers can pass through pores smaller than their own diameter. Increasing the level of surfactant in vesicle membranes brings no advantages in terms of transcutaneous permeation efficiency above a certain concentration. Only an optimum ratio of lipid and surfactant could lead to bilayer flexibility liposomal membranes. Addition of other lipophilic compounds, such as cholesterol sulfate, to lipophilic/amphiphilic bilayers tend to decrease their elasticity, even at low molar concentrations of amphiphilic compounds in the bilayer [19].

To determine the amount of Sit-G incorporated into vesicles, we preliminarily measured the elasticity of preparations containing Tween or Cholate at different concentrations, plus Sit-G at 5% and 10% (w/w). Incorporation of 5% (w/w) Sit-G into Cholate formulations did not decrease their elasticity value (Fig. 2B), but incorporation of 10% (w/w) Sit-G significantly decreased it (data not shown). The absorption enhancing effect exerted by Sit-G could be attributed to its steroidal structure and similarity with cholesterol and Cholate. Incorporation of steroids in fluid vesicle bilayers enhances the degree in molecular ordering or change the compaction of bilayers [20]. Therefore, the addition of 5% (w/w) (6 mol%) Sit-G as a small amount to CS-vesicle bilayers was useful and did not decrease elasticity, but decreases in elasticity might become noticeable at high concentrations of Sit-G.

The strength of interaction between different surfactants in the bilayer was dependent on their molar ratios. At a high molar ratio, Cholate showed greater effect on J_{flux} than Tween, but this difference was limited because the hydrophile–lipophile balance (HLB) of Cholate and Tween was similar [8]. Maximum elasticity of C- and CS-vesicles was seen in 16% (w/w) Cholate, C16 and CS16 preparations. The elasticity of T-vesicles might increase with further addition of Tween, but too much surfactant might cause skin irritation as well as reducing drug entrapment by creating mixed micelles [21]. These mixed micelles have been reported to be less effective in transdermal drug delivery, as compared with ultra-deformable vesicles, because micelles are much less sensitive

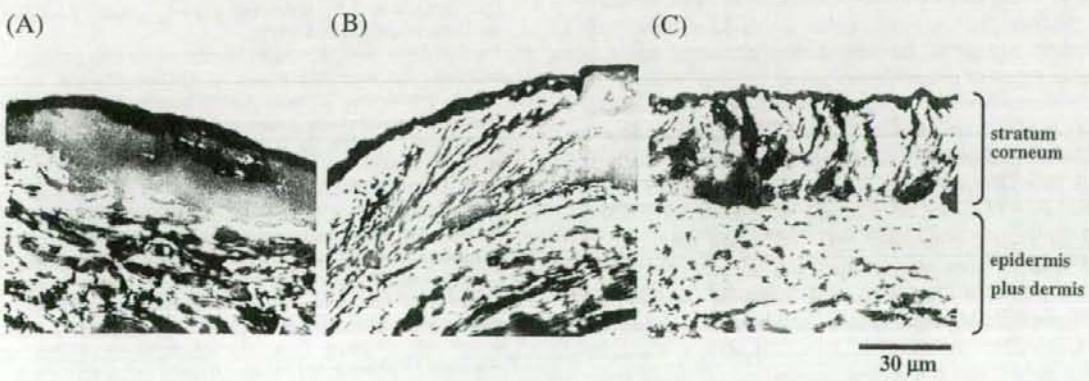

Fig. 8. Optical cross-sections perpendicular to the hairless rat surface incubated with fluorescent-labeled CS16-vesicles. Cross-sectional images were obtained by CLSM following a 3 h-application of CS16-vesicles labeled with DiI and entrapped with calcein (A), a mixture suspension of free calcein and CS16-vesicles labeled with DiI (B), and a mixture solution of free DiI and calcein in 5% ethanol solution (C).

to water activity gradients than ultra-deformable vesicles. Cevc et al. [22] compared the penetration ability of ultra-deformable vesicles (so called Transfersomes), liposomes, and mixed micelles by CLSM and observed that mixed micelles were restricted to the top-most part of stratum corneum whereas Transfersomes penetrated to a deeper skin layer. As a result of high elasticity and low surfactant concentrations, C16-, CS16- and T16-vesicles were chosen as lead formulations for BLM-vesicles.

Preparations of C16-BLM exhibited significantly higher BLM entrapment efficiency than T16- and EPC-BLM vesicles (Table 3). That may be due to electrostatic interaction between negatively-charged Cholate and positively-charged BLM, but also interaction between BLM and Sit-G molecules incorporated into the membrane. It might be one of the reasons why CS16-vesicles obtained a high entrapment efficiency of 28% despite being less negatively-charged than C16-vesicles.

Following topical application onto rats, CS16-BLM delivered significantly higher concentrations of BLM into the skin compared to C16-BLM, EPC-BLM and BLM solutions 3 h after application. Moreover, most of the BLM that had been absorbed was then distributed quickly into the epidermis and dermis. Vesicles enhanced BLM penetration and this may be due to EPC temporarily changing the ultrastructual properties of the skin [23,24]. Furthermore, penetration may be augmented by the deformability of vesicles and the presence of Sit-G.

The superior penetration potential of CS16-vesicles was further confirmed by skin penetration studies performed by CLSM analysis with fluorescent probes of DiI and calcein. CLSM images taken of rat skin after 3 h incubation with fluorescent probes showed that calcein did not penetrate into the skin when applied as a solution, but was transported into the bottom of SC layer when encapsulated in CS16-vesicles. This finding suggests that ultra-deformable vesicles can deliver hydrophilic drugs encapsulated in vesicles.

CS-BLM increased significantly penetration of BLM into viable epidermis and dermis than C-BLM, suggesting that incorporation of Sit-G into vesicles has a strong penetration enhancing effect. This additional effect of the Sit-G incorporated in a vesicle as absorption enhancer could be attributed to its interactions with the SC lipids. Sit-G may have been incorporated into the SC bilayers, thereby increasing the space of polar domains of these bilayers.

The physicochemical background of Sit-G and Cholate has to be taken into consideration. Sit-G is slightly water-soluble and Cholate is soluble. Cholate 0.16% (w/w) aqueous solution may form mixed micelles despite the CMC of Cholate being observed at 6.2 mM, 0.25% (w/w) [25,26]. Ultra-deformable formulations of BLM may compose of various vesicles, such as liposomes and micelles. Under the conditions used in this study, the effect of micelles on permeation of BLM should not be neglected. However, the ratio of liposome to micelles in CS-BLM has not been estimated at the present time. Further studies will therefore be necessary to investigate the effect of various types of vesicles on skin-permeation enhancer properties.

5. Conclusions

Ultra-deformable formulations containing Sit-G increased entrapment efficiency of BLM and maintained in vitro stability and flexibility. Ultra-deformable vesicles incorporating Sit-G and entrapped with BLM, when applied non-occlusively onto rat skin, significantly increased distribution of BLM in epidermis and dermis compared with ultra-deformable vesicles without Sit-G.

Acknowledgements

We greatly acknowledge Dr. Kent G. Lau for his review of the manuscript. This project was supported in part by a grant from The Promotion and Mutual Aid Corporation for Private Schools of Japan, and by a Grant-in-aid for Scientific Research from the Ministry of Education, Culture, Sports, Science, and Technology of Japan.

References

[1] B.W. Barry, S.L. Bennett, Effect of penetration enhancers on the permeation of mannitol, hydrocortisone and progesterone through human skin, J. Pharm. Pharmacol. 39 (1987) 535–546.
[2] K. Tojo, C.C. Chiang, Y.W. Chien, Drug permeation across the skin: effect of penetrant hydrophilicity, J. Pharm. Sci. 76 (1987) 123–126.
[3] A. Sharma, U.S. Sharma, Liposomes in drug delivery: progress and limitations, Int. J. Pharm. 154 (1997) 123–140.
[4] G. Cevc, A. Schatzlein, D. Gebauer, G. Blume, Ultrahighefficiency of drug and peptide transfer through intact skin by means of novel drug carriers, transfersomes, in: K.R. Bain, J. Hadgkraft, W.J. James, K.A. Water (Eds.), Prediction of Percutaneous Penetration, vol. 3b, STS Publishing, Cardiff, 1993, pp. 226–236.
[5] G. Cevc, G. Blume, Lipid vesicles penetrate into intact skin owing to the transdermal osmotic gradients and hydration force, Biochim. Biophys. Acta 1104 (1992) 226–232.
[6] M.E. Planas, P. Gonzalez, L. Rodriguez, S. Sanchez, G. Cevc, Noninvasive percutaneous induction of topical analgesia by a new type of drug carrier, and prolongation of local pain insensitivity by anesthetic liposomes, Anesth. Analg. 75 (1992) 615–621.
[7] G. Cevc, G. Blume, Biological activity and characteristics of triamcinolone-acetonide formulated with the self-regulating drug carriers, transfersomes, Biochim. Biophys. Acta 1614 (2003) 156–164.
[8] G.M. El Maghraby, A.C. Williams, B.W. Barry, Oestradiol skin delivery from ultradeformable liposomes: refinement of surfactant concentration, Int. J. Pharm. 196 (2000) 63–74.
[9] K.G. Lau, S. Chopra, Y. Maitani, Entrapment of bleomycin in ultra-deformable liposomes, S.T.P. Pharma Sci. 13 (2003) 237–239.
[10] K.G. Lau, Y. Hattori, S. Chopra, E.A. O'Toole, A. Storey, T. Nagai, Y. Maitani, Ultra-deformable liposomes containing bleomycin: in vitro stability and toxicity on human cutaneous keratinocyte cell lines, Int. J. Pharm. 300 (2005) 4–12.
[11] K. Muramatsu, Y. Maitani, K. Takayama, T. Nagai, The relationship between the rigidity of the liposomal membrane and the absorption of insulin after nasal administration of liposomes modified with an enhancer containing insulin in rabbits, Drug Dev. Ind. Pharm. 25 (1999) 1099–1105.
[12] K. Nakamura, K. Takayama, T. Nagai, Y. Maitani, Regional intestinal absorption of FITC-dextran 4400 with nanoparticles based on beta-sitosterol beta-D-glucoside in rats, J. Pharm. Sci. 92 (2003) 311–318.
[13] G. Cevc, A. Schatzlein, G. Blume, Transdermal drug carriers: basic properties, optimization and transfer efficiency in the case of epicutaneously applied peptides, J. Control. Release 36 (1995) 3–16.
[14] G. Cevc, D. Gebauer, J. Stieber, A. Schatzlein, G. Blume, Ultraflexible vesicles, transfersomes, have an extremely low pore penetration resistance

and transport therapeutic amounts of insulin across the intact mammalian skin, Biochim. Biophys. Acta 1368 (1998) 201–215.
[15] W.R. Perkins, S.R. Minchey, P.L. Ahl, A.S. Janoff, The determination of liposome captured volume, Chem. Phys. Lipids 64 (1993) 197–217.
[16] H.P. Fiedler, J. Wachter, High-performance liquid chromatographic determination of bleomycins, J. Chromatogr. 536 (1991) 343–347.
[17] A.D. Bangham, M.M. Standish, J.C. Watkins, Diffusion of univalent ions across the lamellae of swollen phospholipids, J. Mol. Biol. 13 (1965) 238–252.
[18] A.D. Bangham, Membrane models with phospholipids, Prog. Biophys. Mol. Biol. 18 (1968) 29–95.
[19] B.A. van den Bergh, P.W. Wertz, H.E. Junginger, J.A. Bouwstra, Elasticity of vesicles assessed by electron spin resonance, electron microscopy and extrusion measurements, Int. J. Pharm. 217 (2001) 13–24.
[20] L.J. Korstanje, G. van Ginkel, Y.K. Levine, Effects of steroid molecules on the dynamical structure of dioleoylphosphatidylcholine and digalactosyldiacylglycerol bilayers, Biochim. Biophys. Acta 1022 (1990) 155–162.
[21] C. Hofer, R. Hartung, R. Gobel, P. Deering, A. Lehmer, J. Breul, New ultradeformable drug carriers for potential transdermal application of interleukin-2 and interferon-alpha: theoretic and practical aspects, World J. Surg. 24 (2000) 1187–1189.
[22] G. Cevc, G. Blume, A. Schatzlein, D. Gebauer, A. Paul, The skin: a pathway for systemic treatment with patches and lipid-based agent carriers, Adv. Drug Deliv. Rev. 18 (1996) 349–378.
[23] A. Blume, M. Jansen, M. Ghyczy, J. Gareiss, Interaction of phospholipid liposomes with lipid model mixtures for stratum corneum lipids, Int. J. Pharm. 99 (1993) 219–228.
[24] H.E. Hofland, J.A. Bouwstra, H.E. Bodde, F. Spies, H.E. Junginger, Interactions between liposomes and human stratum corneum in vitro: freeze fracture electron microscopical visualization and small angle X-ray scattering studies, Br. J. Dermatol. 132 (1995) 853–866.
[25] R. Ninomiya, K. Matsuoka, Y. Moroi, Micelle formation of sodium chenodeoxycholate and solubilization into the micelles: comparison with other unconjugated bile salts, Biochim. Biophys. Acta 1634 (2003) 116–125.
[26] H. Sugioka, K. Matsuoka, Y. Moroi, Temperature effect on formation of sodium cholate micelles, J. Colloid Interface Sci. 259 (2003) 156–162.

Folate-Linked Lipid-Based Nanoparticles Deliver a NFκB Decoy into Activated Murine Macrophage-Like RAW264.7 Cells

Yoshiyuki HATTORI,[a] Makoto SAKAGUCHI,[b] and Yoshie MAITANI*,[a]

[a] *Institute of Medicinal Chemistry, Hoshi University; 2–4–41 Ebara, Shinagawa-ku, Tokyo 142–8501, Japan: and* [b] *AnGes MG, Inc.; 4F, Saito Bio-Incubator, 7–7–15 Saito-asagi, Ibaraki, Osaka 567–0085, Japan.*
Received March 13, 2006; accepted April 20, 2006; published online April 27, 2006

Activated macrophages are the key effector cells in rheumatoid arthritis (RA) and secrete multiple mediators of inflammation including proinflammatory cytokines. We investigated delivery of a nuclear factor kappa B (NFκB) decoy by folate-linked lipid-based nanoparticles (NP-F) into murine macrophages. The expression of folate receptor (FR) in RAW264.7 cells activated by lipopolysaccaride was confirmed by strong expression of FR mRNA, and association of FITC-labeled folate-BSA conjugate. When transfected *via* NP-F, the NFκB decoy was strongly detected in the cytoplasm, and an inhibitory effect on the translocation of NFκB into the nucleus was observed at 0.03 μM of the decoy, suggesting that NP-F effectively delivered the NFκB decoy into the cytoplasm. This information is of value for the design of NFκB decoy carrier systems targeting FR in activated macrophages in gene therapy for autoimmune diseases such as RA.

Key words nuclear factor kappa B (NFκB) decoy; folate receptor; folate-linked nanoparticle; macrophage; rheumatoid arthritis

Activated synovial macrophages are present in large numbers in arthritic joints in autoimmune diseases such as rheumatoid arthritis (RA),[1] and release many proinflammatory cytokines such as tumor necrosis factor-α (TNF-α).[1,2] Nuclear factor kappa B (NFκB) is a transcription factor which normally resides in the cytoplasm, complexed with an inhibitor, IκB, in an inactive form.[3] Proinflammatory cytokines induce a rapid nuclear translocation of NFκB through degradation of IκB, and NFκB interacts with response-associated genes such as TNF-α, and activates their transcription.[2] The decoy technique can block intracellular signaling pathways using a double-stranded oligonucleotide directed at a cognate sequence of NFκB.[3]

Although mannosylated cationic liposomes can deliver genes to macrophages,[4,5] the target of the NFκB decoy is activated macrophages; therefore, activated macrophage-selective gene targeting is of great importance. A functionally active folate receptor (FR)-β was detected in activated synovial macrophages,[6] and was utilized a folate-linked imaging agent[7] and FR-β antibody conjugates.[8] However, gene delivery with folate-linked vectors into activated macrophages has not been reported.

Previously, we reported that folate-linked lipid-based nanoparticles (NP-F) delivered DNA with selectively high transfection efficiency into the FR expressed cells.[9] In the present study, we examined the efficiency of the transfection of NP-F into activated murine macrophage-like RAW264.7 cells treated with lipopolysaccaride (LPS) by investigating the intracellular distribution of a NFκB decoy using confocal microscopy. Furthermore, to examine the ability of the decoy to inhibit the translocation of NFκB into the nucleus, the amount of NFκB in the nucleus was determined by ELISA after transfection with the NFκB decoy *via* NP-F.

MATERIALS AND METHODS

Materials The NFκB decoy oligonucleotide used in this study is a 20-mer phosphorothioate double-stranded oligonucleotide, 5′-CCTTGAAGGGATTTCCCTCC-3′. LPS from *E. coli* 111:B4 was purchased from Wako Pure Chemicals (Osaka, Japan). 3([*N*-(*N*′,*N*′-dimethylaminoethane)-carbamoyl]cholesterol (DC-Chol) was purchased from Sigma Chemical Co. (St. Louis, MO, U.S.A.). Tween 80 was supplied by NOF Co. Ltd. (Tokyo, Japan). All reagents were of analytical grade. DMRIE-C reagent, folate deficient-RPMI1640 medium and fetal bovine serum (FBS) were purchased from Invitrogen Co. (Carlsbad, CA, U.S.A.).

Cell Culture RAW 264.7 cells were supplied by Riken Cell Bank (Ibaraki, Japan). The cells were grown in a folate-deficient RPMI-1640 medium supplemented with 10% heat-inactivated FBS and kanamycin (100 μg/ml) at 37 °C in a 5% CO_2 humidified atmosphere.

RT-PCR Analysis of FR Expression in RAW 264.7 Cells Cells were incubated with or without 100 ng/ml of LPS in medium for 4 h. Total RNA was isolated from the cells and RT-PCR was performed as described previously.[9] For the amplification of mouse FR-α, the primers FR-α-FW, 5′-AGGACTGAACTTCTCAATGTCTGCATGG-3′, and FR-α-RW, 5′-GCTTGTAGGAGTGACTCCAGATTTCCTC-3′, were used. For the amplification of mouse FR-β, the primers FR-β-FW, 5′-CAAGCTGCATGACCAGTGTAGTCCATGG-3′, and FR-β-RW, 5′-ATCTGGATGCAGCGGCCACTCCCTCTGC-3′, were used. For the amplification of mouse β-actin, the primers β-actin-FW, 5′-ACCCACACTGTGCCCATCTA-3′, and β-actin-RW, 5′-CTGCTTGCTGATCCACATCT-3′, were used. The PCR products for FRs and β-actin were analyzed by 1.5% agarose gel electrophoresis in a Tris-Borate-EDTA (TBE) buffer. The products were visualized by ethidium bromide staining.

Real time PCR was performed on the corresponding cDNA synthesized from each sample described above. The optimized settings were transferred to real time PCR protocols on iCycler MyiQ detection systems (Bio-Rad Laboratories, Hercules, CA, U.S.A.) and SYBR Green I assay (iQ™ SYBER Green Supermix, Bio-Rad Laboratories) was used for quantification. Samples were run in triplicate and the expression level of FR-α mRNA was normalized for the amount of β-actin in the same sample. Difference of 1 cycle

* To whom correspondence should be addressed. e-mail: yoshie@hoshi.ac.jp

was calculated as a 2 fold-change in the gene expression.

Association of a FITC-Labeled Folate-Bovine Serum Albumin Conjugate Synthesis of a FITC-labeled folate-BSA conjugate (FITC-f-BSA) was carried out as previously described.[9] Cells were plated into 35-mm culture dishes, and were treated with 100 ng/ml of LPS for 4 h before the experiment. FITC-f-BSA was diluted to 10 μM in 1 ml of folate-deficient RPMI medium containing 10% serum and then incubated with the cells in the presence or absence of 1 mM folic acid. After 30 min of incubation, the cells were washed twice with PBS (pH 7.4) to remove the unbound FITC-f-BSA and fixed with 10% formaldehyde in PBS for 15 min at room temperature. For staining the nucleus, the fixed cells were washed and incubated with 0.5 mg/ml of RNase in PBS for 10 min at 37 °C. Subsequently, the cells were washed and incubated with propidium iodide (PI) for 10 min at room temperature. FITC-f-BSA and PI were visualized with a Radiance 2100 confocal laser scanning microscope (Bio-Rad Laboratories) as previously described.[9]

Preparation of Folate-Linked Nanoparticles Folate-polyethyleneglycol-distearoylphoshatidylethanolamine (f-PEG_{2000}-DSPE, mean molecular weight of PEG: 2000 Da) was synthesized as previously described.[10] NP-F was prepared with lipids (DC-Chol : Tween 80 : f-PEG_{2000}-DSPE = 93 : 5 : 2, molar ratio = 10 : 1.3 : 1.3 mg) in 10 ml of water by a modified ethanol injection method as described previously.[9] NP-F formed nanoplex of about 200 nm, and even in the presence of serum, maintained its size (about 400 nm).[9]

Transfection Based on a preliminary assay of the inhibition of NFκB activation, the optimized total concentration of lipid in NP-F and DMRIE-C was determined as 60 μg/ml. For the transfection with NP-F, the NFκB double-stranded decoy was diluted to 20, 60, 200 and 2000 μM, and a single-stranded decoy was diluted to 400 and 4000 μM with medium. A complex (NP-F nanoplex) was formed by adding the decoy (3.6 μl of 20, 60, 200, 2000 μM double-stranded decoy and 400 and 4000 μM single-stranded decoy, respectively) to the NP-F solution (17.1 μl), mixing with gentle shaking, and leaving the mixture at room temperature for 15 min. The mixture was added to 3.6 ml of medium, and 1 ml was then added to 1 ml of cell culture in a 35-mm culture dish. The transfection with DMRIE-C was performed according to the manufacturer's instructions.

Intracellular Distribution of the NFκB Decoy Cells were plated into 35-mm culture dishes, and treated with or without 100 ng/ml of LPS for 2 h before the experiment. The NP-F nanoplex or DMRIE-C lipoplex was formed with the FITC-labeled NFκB decoy as described above and then diluted in 3.6 ml of medium. The mixtures (1 ml) were added to 1 ml of cell culture and incubated with the cells for 4 h in the presence of 100 ng/ml of LPS. After the incubation, the cells were fixed with 10% formaldehyde and incubated with PI for staining of the nucleus as described above. Examinations were performed with the confocal laser scanning microscope.

Measurement of the Amount of NFκB in the Nucleus Cells were transfected with either the double- or single-stranded decoy using NP-F or the DMRIE-C reagent, and incubated for 4 h in the medium without LPS and then treated with 100 ng/ml of LPS for 1 h. The activation of p65, a transcription factor of the NFκB family, was analyzed using a TransAM assay kit according to the manufacturer's directions (Active Motif Europe, Rixensart, Belgium). Briefly, the LPS-treated cells were scraped off and centrifuged for 10 min at 1000 rpm. The pellet was suspended in 100 μl of hypotonic buffer and 5 μl of detergent, and was centrifuged for 30 s at 14000 ***g***. The pellet was resuspended in 20 μl of lysis buffer, incubated for 30 min at 4 °C, and centrifuged for 10 min at 14000 ***g***. The supernatant constitutes the cell extract. Cell extract from each sample was diluted 5 times and incubated in 96-well plates coated with the NFκB consensus double-stranded oligonucleotide sequence (5′-AGTTGAGGGGAC-TTTCCCAGGC-3′) for 1 h. Bound p65 was detected with rabbit anti-mouse p65 antibody and peroxidase-conjugated anti-rabbit IgG antibody. After a colorimetric reaction, the optical density was read at 450 nm.

Cytotoxicity The cytotoxicity upon transfection using NP-F or DMRIE-C was evaluated with a cell proliferation assay kit (Dojindo, Kumamoto, Japan). Cells were placed in a 24-well plate in the medium containing serum, and were transfected with the double-stranded NFκB decoy at 0.1 and 1 μM or single-stranded NFκB decoy at 2 μM *via* NP-F or DMRIE-C. After 24 h of incubation, the medium was removed, and the cells were treated with a WST-8 (2-(2-methoxy-4-nitrophenyl)-3-(4-nitrophenyl)-5-(2,4-disulfophenyl)-2*H*-tetrazolium, monosodium salt) solution (20 μl) in medium containing 10% FBS (200 μl) for 1 h. Cell viability was expressed relative to the absorbance at 450 nm of untreated cells.

Statistical Analysis The statistical significance of the data was evaluated with the Dunnett test. A p value of 0.05 or less was considered significant.

RESULTS AND DISCUSSION

One major problem in gene therapy is how to transfect target cells efficiently and specifically. First, to investigate the possibility of a FR-based macrophage-targeting therapy, we examined the expression of FR in RAW264.7 cells. RT-PCR analysis of FR-α and β mRNA was done using total RNA from RAW264.7 cells with or without LPS treatment. The unstimulated cells with LPS expressed FR-α mRNA weakly, and FR-β mRNA not at all (Fig. 1A). However, RAW264.7 cells activated by LPS strongly expressed the FR-α mRNA, but did not express the FR-β mRNA (Fig. 1A). FR-α mRNA was increased about 4-fold in the cells by LPS-treatment (Fig. 1B). This suggested that folic acid could be utilized to target activated RAW264.7 macrophages *via* FR-α. Paulos *et al.* reported that in human macrophages from healthy individuals, FR-β was detected immunologically on the surface, but was found to be functionally inactive.[7] They also showed that the FR-β on activated cells can bind folate-linked compounds with high affinity.[6,7] In our study, we found a difference in the expression of the FR isoforms between human RA macrophages and murine RAW264.7 cells. The differences between human primary and murine macrophage-like cell lines can not be compared directly, but it is possible that FR has important roles in the activation of macrophages.

To examine the selectivity of the folate moiety in the uptake into RAW264.7 cells, the intracellular distribution of FITC-f-BSA was visualized by confocal microscopy. The NP-F nanoplex had a positive ζ-potential (about 30—

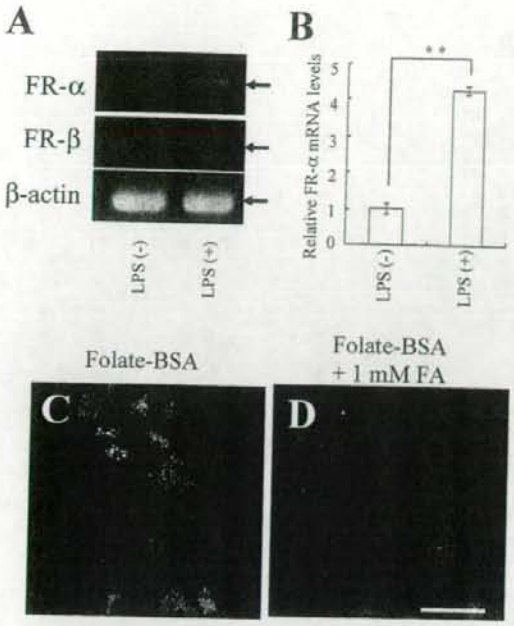

Fig. 1. (A) FR-α, FR-β and β-Actin mRNA Expression was Detected in RAW264.7 Cells with or without LPS Treatment by RT-PCR and (B) Relative Amount of FR-α mRNA in the Cells with or without LPS Treatment was Compared by an SYBR Green I-Based Quantitative PCR Analysis

The *y*-axis indicated the fold induction of gene expression. The expression level of FR-α mRNA was normalized for the amount of β-actin in the same sample. Each result represents the mean±S.D. (n=3). **p<0.01, compared with LPS(−).

(C and D) Association of FITC-f-BSA with RAW264.7 Cells

Cells were treated with 100 ng/ml of LPS for 4 h. After the treatment, FITC-f-BSA was incubated with the cells for 30 min in the absence (C) or presence (D) of 1 mM free folic acid. The FITC-f-BSA was visualized by confocal microscopy (magnification×600). The red signals show the location of the nucleus, and the green signals, that of the FITC-f-BSA. Scale bar=50 μm.

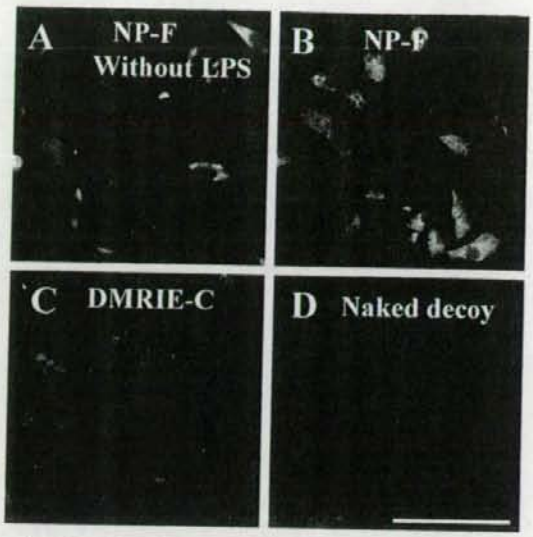

Fig. 2. Comparison of the Intracellular Distribution of the FITC-Labeled NFκB Decoy between NP-F and DMRIE-C Transfection

In (A), RAW264.7 cells were transfected with NP-F nanoplex of 0.1 μM NFκB decoy and incubated for 4 h without LPS. In (B)–(D), the cells were pretreated with 100 ng/ml of LPS for 2 h. After the pretreatment, the cells were transfected with NP-F nanoplex of 0.1 μM NFκB decoy (B), DMRIE-C lipoplex of 0.1 μM NFκB decoy (C), and 1 μM naked NFκB decoy (D), respectively, and incubated for 4 h in the presence of LPS. The FITC-labeled NFκB decoy was visualized by confocal microscopy (magnification×1200). The red signals show the location of the nucleus, and the green signals, that of the FITC-labeled NFκB decoy. Scale bar=50 μm.

40 mV).[9] It was reported that a negatively charged folic acid formed a charge-mediated complex with positively charged particles through its carboxyl groups and increased non-specifically the efficiency of transfection.[11] In NP-F, we observed that the addition of folic acid into culture medium decreased non-specifically the efficiency of transfection by interaction between positively charged NP-F and folic acid (data not shown). Therefore, we prepared FITC-f-BSA and incubated it with LPS-stimulated or unstimulated RAW264.7 cells in the absence or presence of 1 mM folic acid. The amount of FICT-f-BSA associated with the cells increased on LPS treatment (data not shown). The presence of 1 mM folic acid caused a significant decrease in the amount of FICT-f-BSA associated with the LPS-stimulated cells (Figs. 1C, D). These results indicated that the folate moiety promoted the association of FITC-f-BSA with LPS-stimulated RAW264.7 cells, suggesting that FR can be utilized for targeting activated macrophages.

Next, we examined the localization of the FITC-labeled NFκB decoy after transfection *via* NP-F into RAW264.7 cells. In the unstimulated cells, the FITC-signal was moderately strong in the cytoplasm of a few cells (Fig. 2A). In the LPS-stimulated cells, it was detected throughout the cytoplasm strongly and diffusively in most of the cells (Fig. 2B). This might suggest that the FITC-labeled NFκB decoy nanoplex was efficiently delivered into the cells, was released from the nanoplex, and diffused into the cytoplasm. These results suggested that the association of the FITC-labeled NFκB decoy with the activated macrophages occurred *via* FR and that NP-F was able to deliver the decoy into the cytoplasm of activated macrophages. This *in vitro* distribution of the NFκB decoy observed in RAW 264.7 cells agreed with that reported by Higuchi *et al.*, showing that most of the fluorescent-labeled NFκB decoy was observed in the cytoplasm when transfected by cationic liposomes into RAW264.7 cells stimulated with LPS.[12] DMRIE-C reagent is a liposomal formulation of the cationic lipid DMRIE composed of 1,2-dimyristyloxypropyl-3-dimethyl-hydroxy ethyl ammonium bromide and cholesterol at 1 : 1 (M/M). It is known to be suitable for the transfection of DNA into suspended cells and other lymphoid-derived cell lines. When the ability to carry genes into LPS-stimulated RAW264.7 cells was compared between NP-F and the DMRIE-C reagent, the intracellular distribution of the FITC-labeled NFκB decoy transfected with DMRIE-C was much weaker than that obtained with NP-F in the cytoplasm (Fig. 2C). In the case of the naked NFκB decoy, little intracellular localization was observed in the cells (Fig. 2D).

To examine the ability of the decoy to inhibit the translocation of NFκB into the nucleus after the stimulation by LPS, the amount of NFκB in the nucleus was determined by ELISA after transfection with the NFκB decoy *via* either NP-F or the DMRIE-C reagent. Following LPS treatment, the amount of NFκB in the nucleus was greater when the single-stranded decoy as a control was transfected by either NP-F or DMRIE-C into the cells (Fig. 3A), suggesting that this